TP53-mediated clonal hematopoiesis confers increased risk for incident peripheral artery disease

Seyedeh M. Zekavat BS[1-4]*, Vanesa Viana-Huete PhD[5]*, Saman Doroodgar Jorshery MD MPH[3,6,7], María A. Zuriaga PhD[5], Md Mesbah Uddin PhD[3,4], Mark Trinder BS[3,4,8], Kaavya Paruchuri MD[3,4,9], Nuria Matesanz PhD[5], Virginia Zorita BS MSc[5], Alba Ferrer-Pérez BS MSc[5], Marta Amorós-Pérez BS MSc[5], Scott M. Damrauer MD[10], Christie M. Ballantyne MD[1] , Abhishek Niroula PhD[3,12], Christopher J. Gibson MD[12], James Pirruccello MD[3], Gabriel Griffin MD[13], Benjamin L. Ebert MD PhD[14], Peter Libby MD PhD[7], Valentín Fuster MD PhD[5,15], Hongyu Zhao PhD[16], Marzyeh Ghassemi PhD[6,7], Pradeep Natarajan MD MMSc[3,4,7§], Alexander G. Bick MD PhD[3,17§], José J Fuster PhD[5,18§], Derek Klarin MD[3,19,20§]

1. Yale School of Medicine, New Haven, CT;
2. Computational Biology & Bioinformatics Program, Yale University, New Haven, CT, USA;
3. Program in Medical and Population Genetics, Broad Institute of MIT and Harvard, Cambridge, MA, USA;
4. Cardiovascular Research Center, Massachusetts General Hospital, Boston, MA, USA;
5. Centro Nacional de Investigaciones Cardiovasculares (CNIC), Madrid, Spain;
6. Department of Computer Science, University of Toronto, Toronto, Canada;
7. Department of Electrical Engineering and Computer Science and Institute for Medical and Evaluative Sciences, Massachusetts Institute of Technology, Cambridge, MA;
8. Center for Heart Lung Innovation, University of British Columbia, Vancouver;
9. Department of Medicine, Harvard Medical School, Boston, MA, USA;
10. Department of Surgery, Perelman School of Medicine, University of Pennsylvania, Philadelphia, PA, USA;
11. Center for Cardiometabolic Disease Prevention, Baylor College of Medicine, Houston, TX, USA;
12. Department of Medical Oncology, Dana-Farber Cancer Institute, Boston, MA, USA;
13. Department of Pathology, Brigham and Women's Hospital, Boston, MA, USA;
14. Department of Hematology, Brigham and Women's Hospital, Boston, MA, USA;
15. Icahn School of Medicine at Mount Sinai, New York, NY, USA;
16. Department of Biostatistics, Yale School of Public Health, New Haven, CT;
17. Division of Genetic Medicine, Department of Medicine, Vanderbilt University Medical Center, TN, USA;
18. CIBER en Enfermedades Cardiovasculares (CIBER-CV), Madrid, Spain;
19. Malcolm Randall VA Medical Center, Gainesville, FL;
20. Division of Vascular Surgery, University of Florida College of Medicine, FL, USA

* Co-first authors
§ Equally supervised this work

Corresponding Authors:
Jose J. Fuster, PhD
jjfuster@cnic.es
Melchor Fernández Almagro, 3
28029 - Madrid (Spain)
Tel: (+34) 914531200, ext 4304
Fax: (+34) 914531265
Twitter: @josejfuster
ORCID: 0000-0002-5970-629X

Derek Klarin, MD
derek.klarin@surgery.ufl.edu
1600 SW Archer Road, NG-45, PO Box 100128, Gainesville, FL 32610

Tel: 352-273-5485
Fax: 352-273-5515
ORCID: 0000-0002-4636-5780

_____

Main Text Total word count: 3,517

Funding: P.N. is supported by a Hassenfeld Scholar Award from the Massachusetts General Hospital, grants from the National Heart, Lung, and Blood Institute (R01HL1427, R01HL148565, and R01HL148050), and from Fondation Leducq (TNE-18CVD04). S.M.Z is supported by the NIH National Heart, Lung, and Blood Institute (1F30HL149180-01) and the NIH Medical Scientist Training Program Training Grant (T32GM136651). A.G.B. is supported by a Burroughs Wellcome Fund Career Award for Medical Scientists, a NIH Director Early Independence Award (DP5-OD029586) and a NHLBI BioData Catalyst Fellowship (OT3 HL147154-01). J.P.P is supported by a John S LaDue Memorial Fellowship. K.P. is supported by NIH grant 5-T32HL007208-43. J.J.F. is supported by grants RYC-2016-20026 and RTI2018-093554-A-I00) from the Spanish "Ministerio de Ciencia e Innovación", a 2019 Leonardo Grant for Researchers and Cultural Creators from the BBVA Foundation, the European Research Area Network on Cardiovascular Diseases CHEMICAL (grant AC19/00133 from the "Spanish Instituto de Salud Carlos III") and the Leducq Foundation (TNE-18CVD04). The project leading to these results received funding from "la Caixa" Foundation (ID 100010434), under agreement HR17-00267. The Centro Nacional de Investigaciones Cardiovasculares (CNIC) is supported by the Instituto de Salud Carlos III (ISCIII), the Ministerio de Ciencia e Innovación and the Pro CNIC Foundation. P.L. receives funding support from the National Heart, Lung, and Blood Institute (1R01HL134892), the American Heart Association (18CSA34080399), the RRM Charitable Fund, and the Simard Fund.

Disclosures: P.N. reported grants from Amgen during the conduct of the study and grants from Boston Scientific; grants and personal fees from Apple; personal fees from Novartis and Blackstone Life Sciences; and spousal employment at Vertex all outside the submitted work. P.L. is an unpaid consultant to, or involved in clinical trials for Amgen, AstraZeneca, Baim Institute, Beren Therapeutics, Esperion, Therapeutics, Genentech, Kancera, Kowa Pharmaceuticals, Medimmune, Merck, Norvo Nordisk, Merck, Novartis, Pfizer, Sanofi-Regeneron. Dr. Libby is a member of scientific advisory board for Amgen, Corvidia Therapeutics, DalCor Pharmaceuticals, Kowa Pharmaceuticals, Olatec Therapeutics, Medimmune, Novartis, and XBiotech, Inc. P.L.'s laboratory has received research funding in the last 2 years from Novartis, he is on the Board of Directors of XBiotech, Inc, and has a financial interest in Xbiotech, a company developing therapeutic human antibodies. These interests were reviewed and are managed by Brigham and Women's Hospital and Partners HealthCare in accordance with their conflict of interest policies. The other authors do not report any disclosures.

Acknowledgments: Thanks to the participants and staff of the UK Biobank and Mass General Brigham Biobank. UK Biobank analyses were conducted using Application 7089. Thanks to Dr. Zeyan Liew and teaching fellow Jiajun Lu, the instructors of the causal inference course at Yale.

Abbreviations: CHIP, clonal hematopoiesis of indeterminate potential; PAD, peripheral artery disease

Abstract

Background: Somatic mutations in blood indicative of clonal hematopoiesis of indeterminate potential (CHIP), particularly in *DNMT3A*, *TET2*, and *JAK2*, are associated with an increased risk of hematologic malignancy, coronary artery disease, and all-cause mortality. However, whether CHIP is associated with increased risk of peripheral artery disease (PAD) remains unknown. In addition, chemotherapy frequently causes mutations in DNA Damage Repair (DDR) genes *TP53* and *PPM1D*, and whether CHIP caused by somatic mutations in DDR genes results in increased risk of atherosclerosis is unclear. We sought to test whether CHIP, and CHIP caused by DDR genes, associates with incident peripheral artery disease (PAD) and atherosclerosis.

Methods: We identified CHIP among 50,122 exome sequences in individuals from UK and Mass General Brigham Biobanks and tested CHIP status (N=2,851) with incident PAD and atherosclerosis across multiple arterial beds. To mimic the human scenario of clonal hematopoiesis and test whether the expansion of p53-deficient hematopoietic cells contributes to atherosclerosis, a competitive bone marrow transplantation (BMT) strategy was used to generate atherosclerosis-prone *Ldlr*-/- chimeric mice carrying 20% *Trp53*-/- hematopoietic cells (20% KO-BMT mice). We then evaluated aortic plaque burden and plaque macrophage accumulation 12 weeks after grafting.

Results: CHIP associated with incident PAD (HR 1.7; $P=2.2x10^{-5}$) and atherosclerosis in multiple beds (HR 1.3; $P=9.7x10^{-5}$), with increased risk among individuals with DDR CHIP (HR 2.0; P=0.0084). Among atherosclerosis-prone *Ldlr* null mice, the p53 -/- 20% KO-BMT mice demonstrated increased aortic plaque size (p=0.013) and accumulation of p53-/- plaque macrophages (P<0.001), driven by an abundance of p53-deficient plaque macrophages. The

expansion of p53-deficient cells did not affect the expression of the pro-inflammatory cytokines IL-6 and IL-1β in the atherosclerotic aortic wall.

Conclusions: Our findings highlight the role of CHIP as a broad driver of atherosclerosis across the entire arterial system, with evidence of increased plaque among p53 -/- 20% KO-BMT mice via expansion of plaque macrophages. These observations provide new insight into the link between CHIP and cardiovascular disease, and lend human genetic support to the concept that post-cytotoxic chemotherapy patients may benefit from surveillance for atherosclerotic conditions in addition to therapy-related myeloid neoplasms.

Abstract Word Count: 346

Key Words: somatic, atherosclerosis, clonal hematopoiesis, sequencing

143 **Introduction**

144 Peripheral artery disease (PAD) is a leading cause of cardiovascular morbidity and mortality
145 worldwide, and age is among its strongest risk factors. PAD associates with an extremely high
146 cardiovascular mortality and unmitigated can progress to limb loss[1]. The age-related acquisition
147 and expansion of leukemogenic mutations in hematopoietic stem cells has recently been
148 associated with an increased risk of hematologic malignancy, coronary artery disease, and
149 overall mortality[2, 3]. This phenomenon, termed clonal hematopoiesis of indeterminate potential
150 (CHIP), is relatively common in asymptomatic older adults, affecting at least 10% of individuals
151 older than 70 years of age[4]. CHIP mutations most frequently occur in epigenetic regulators
152 *DNMT3A* and *TET2,* in DNA damage repair (DDR) genes *PPM1D* and *TP53*, or cell cycle and
153 transcriptional regulator genes *JAK2* and *ASXL1*[5]. CHIP associates with coronary artery disease
154 in multiple studies[2, 6]. Whether CHIP links with increased risk of atherosclerosis in the peripheral
155 arterial bed (PAD) is unknown.

156 Here, we leveraged 50,122 whole exome sequences from two genetic biobanks (UK
157 Biobank [UKB], Mass General Brigham Biobank [MGBB]) and tested whether CHIP was
158 associated with increased risk of PAD and atherosclerosis across multiple arterial beds, and
159 additionally whether these associations varied by putative CHIP driver gene. Based on these
160 results, we then performed functional analyses in *Ldlr*-null mice transplanted with 20% *Trp53*-/-
161 bone marrow cells, a murine model of atherosclerosis and clonal hematopoiesis driven by *TP53*
162 mutations.

163

164 **Methods**

165 *Cohorts and exclusion criteria*

166 The UKB is a population-based cohort of approximately 500,000 participants recruited from
167 2006-2010 with existing genomic and longitudinal phenotypic data and median 10-year follow-
168 up[7]. Baseline assessments were conducted at 22 assessment centres across the UK with sample
169 collections including blood-derived DNA. Of ~49,960 individuals with WES data available, we
170 analyzed 37,657 participants consenting to genetic analyses after our exclusion criteria. Use of
171 the data was approved by the Massachusetts General Hospital Institutional Review Board
172 (protocol 2013P001840) and facilitated through UK Biobank Application 7089.
173 The MGBB contains genotypic and clinical data from >105,000 patients who consented
174 to broad-based research across 7 regional hospitals and median 3-year follow-up[8]. Baseline
175 phenotypes were ascertained from the electronic medical record and surveys. We analyzed
176 12,465 individuals consenting to genetic analysis after our exclusion criteria. Use of the data was
177 approved by the Massachusetts General Hospital Institutional Review Board (protocol
178 2020P000904).
179 Across both cohorts, we excluded individuals with prevalent hematologic cancer,
180 individuals without genotypic-phenotypic sex concordance, and one of each pair of 1st or 2nd
181 degree relatives at random. For the UKB, samples were further restricted to individuals with
182 Townsend deprivation index, a marker of socioeconomic status, available for analysis. Follow-up
183 time was defined as time from enrollment to disease diagnosis for cases, or to censorship or
184 death for controls.
185
186 *Whole exome sequencing and CHIP calling*
187 UKB WES were generated from whole blood-derived DNA at the Regeneron Sequencing
188 Center[9]. MGBB WES were generated using whole blood-derived DNA using Illumina

189 sequencing (mean coverage 55x). Somatic CHIP variants were detected with GATK MuTect2
190 software with parameters as previously described[6, 10]. Common germline variants and sequencing
191 artifacts were excluded as before. Samples were annotated with the presence of any CHIP if
192 MuTect2 identified one or more of a pre-specified list of pathogenic somatic variants, as
193 previously described[11, 12]. Additionally, samples were annotated with the presence of Large
194 CHIP (variant allele frequency >10%), as larger CHIP clones have previously been more
195 strongly associated with adverse clinical outcomes[6].
196
197 *Phenotype definitions*
198 Across both UKB and MGBB, PAD was defined by grouping together ICD-10 and ICD-9 billing
199 codes for aortic atherosclerosis (I70), peripheral vascular disease (I73.8, I73.9), and operative
200 procedures including amputation of leg (X09.3-5), bypass of artery of leg (L21.6, L51.3, L51.6,
201 L51.8, L59.1-8), endarterectomy or angioplasty of leg artery (L52.1-2, L54.1,4,8, L60.1-2,
202 L63.1,5), and other transluminal operations on leg arteries or peripheral stent placement
203 (L63.9,L66.7), as previously described[13]. Additionally, in the UKB self-reported peripheral
204 vascular disease, leg claudication/intermittent claudication, arterial embolism, femoral-popliteal
205 leg artery bypass, leg artery angioplasty +/- stent, or amputation of leg were also incorporated
206 (Data fields 20002, 20004) as performed previously[13]. Coronary artery disease and cerebral
207 atherosclerosis phenotype definitions for each cohort are detailed in **Tables I and II in the**
208 **supplement**. Other atherosclerotic conditions were defined using the Phecode Map 1.2[14] ICD-9
209 (https://phewascatalog.org/phecodes) and ICD-10 (https://phewascatalog.org/phecodes_icd10)
210 phenotype groupings for "abdominal aortic aneurysm", "aortic aneurysm", "other aneurysm",
211 "chronic vascular insufficiency of intestine", "acute vascular insufficiency of intestine",

212 “atherosclerosis of renal artery”. The composite atherosclerosis phenotype was created by
213 combining all analyzed atherosclerosis phenotypes (including PAD, coronary artery disease,
214 cerebral atherosclerosis, abdominal aortic aneurysm, aortic aneurysm, other aneurysm, chronic
215 vascular insufficiency of intestine, acute vascular insufficiency of intestine, and atherosclerosis
216 of renal artery) into one phenotype, whereby the first instance across all of these phenotypes was
217 used to determine time of first diagnosed atherosclerotic disease for survival analysis. Other
218 phenotypic covariates (never/prior/current smoking status, hypertension, hyperlipidemia,
219 principal components of ancestry, etc.) were used as previously defined[15].
220
221 *Association Analysis*
222 In the UKB and MGBB a traditional cox-proportional hazards model was utilized using the
223 Survival package in R-3.5 adjusting for age, age^2, sex, smoking status, normalized Townsend
224 deprivation index as a marker of socioeconomic status (only available in UKB), and the first ten
225 principal components of genetic ancestry. Demographic and clinical characteristics found to
226 differ between individuals with and without CHIP were tested using chi-squared (categorical)
227 and Wilcoxon-rank sum (continuous) tests with a two-tailed $P< 0.05$ determining significance.
228 Sensitivity analysis including other covariates (normalized BMI, prevalent hypertension,
229 prevalent Type 2 diabetes, and prevalent hyperlipidemia) was not found to significantly change
230 associations with PAD in the UKB (**Figure I in the supplement**). Additional sensitivity
231 analyses were utilized in the UKB including propensity score adjustment, as well as a marginal
232 structural cox proportional hazards model estimated through stabilized inverse-probability-
233 treatment-weight (IPTW)[16] to estimate the total causal effect of CHIP on PAD. Further details of
234 propensity score methods and stabilized IPTW analysis are described in the supplementary

235 appendix. For our primary outcome PAD, results were combined across the UKB and MGBB
236 using an inverse-variance weighted fixed effects meta-analysis, a two tailed association $P < 0.05$
237 determined statistical significance. In our secondary analysis of CHIP with 10 additional,
238 incident atherosclerotic diseases, a two-tailed Bonferroni p-value threshold of $P<0.05/10=0.005$
239 was used to declare statistical significance.
240
241 *Mice*
242 Animal experiments followed protocols approved by the Institutional Ethics Committee
243 at the Centro Nacional de Investigaciones Cardiovasculares and conformed to EU Directive
244 86/609/EEC and Recommendation 2007/526/EC regarding the protection of animals used for
245 experimental and other scientific purposes, enforced in Spanish law under Real Decreto
246 1201/2005. All mice were maintained on a 12-h light/dark schedule in a specific pathogen-free
247 animal facility in individually ventilated cages and given food and water ad libitum. C57Bl/6J
248 *Trp53*-/- mice were obtained from the Jackson Laboratory. *Ldlr*-/- mice carrying the CD45.1
249 isoform of the CD45 hematopoietic antigen were generated by crossing LDLR-KO mice from
250 the Jackson Laboratory and B6.SJL-*PtprcaPepcb*/BoyCrl mice from Charles River Laboratories.
251 *Competitive bone marrow transplantation and atherosclerosis induction in mice*
252 CD45.1+ *Ldlr*-/- recipients were transplanted with suspensions of BM cells containing 20%
253 CD45.2+ *Trp53*-/- cells and 80% CD45.1+ *Trp53*+/+ cells (20% KO-BMT mice) or 20 %
254 CD45.2+ *Trp53*+/+ cells and 80% CD45.1+ *Trp53*+/+ cells (20% WT-BMT mice) similar to
255 previous studies[17] (**Figure II in the supplement**). BM cells were isolated from femurs and tibias
256 of donor mice after euthanasia. Recipient *Ldlr*-/- mice were exposed to two doses of 450 rad
257 three hours apart. After the second irradiation, each recipient mouse was injected

258 with 10^7 BM cells i.v. Water was supplemented with antibiotics for 7 days before transplant and
259 for 14 days post-transplant. Mice that did not recover full pre-irradiation body weight 28 days
260 after transplant were excluded from further analysis. Starting four weeks after BMT, mice were
261 fed a high fat high cholesterol (HF/HC) Western diet (Harlan-Teklad, TD.88137, Adjusted
262 Calories Diet; 42% from fat, 0.2% cholesterol) to promote hypercholesterolemia and the
263 development of atherosclerosis. Mice were maintained on a HF/HC diet for 9 weeks
264
265 *Quantification of aortic atherosclerosis burden in mice*
266 Mice were euthanized and aortas were removed after in situ perfusion with phosphate-buffered
267 saline injected through the left ventricle of the heart. Tissue fixation was achieved by immersion
268 in 4% paraformaldehyde in PBS overnight at 4°C. Aortic tissue was then dehydrated and
269 embedded in paraffin for sectioning. Histological sections comprising the aortic root as
270 determined by the location of the aortic valve leaflets were cut at a thickness of 4 μm or 6 μm.
271 An operator who was blinded to genotype quantified plaque size in aortic root sections by
272 computer-assisted morphometric analysis of microscopy images. For each mouse, atherosclerotic
273 plaque size in aortic root cross-sections was calculated as the average of 5 independent sections
274 separated by ~16μm. Atherosclerotic plaque composition was examined by
275 immunohistochemical techniques. Vascular smooth muscle cells were identified with an alkaline
276 phosphatase-conjugated mouse anti-smooth muscle α-actin (SMA) monoclonal antibody (clone
277 1A4, SIGMA) and Vector Red Alkaline Phosphatase Substrate (Vector Laboratories).
278 Macrophages were detected with a rabbit anti-Mac2 monoclonal antibody (Santa Cruz
279 Biotechnologies), a biotin-conjugated goat anti-rat secondary antibody and streptavidin-HRP,
280 DAB substrate (all from Vector Laboratories), with hematoxylin counterstaining. Collagen

281 content was determined by a modified Masson's trichrome staining. Microscopy images were
282 analyzed using ImageJ software using the Color Deconvolution plugin. Plasma was collected in
283 EDTA-coated tubes and cholesterol levels were determined using an enzymatic assay
284 (Cholesterol E, WAKO Diagnostics).
285
286 *Flow cytometry analyses of blood and tissue samples.*
287 Peripheral blood was obtained from the facial vein and collected into EDTA-coated tubes. Bone
288 marrow cells were flushed out of two femurs and two tibias per mouse. Aortic arches were
289 digested for 45 minutes at 37°C in RPMI containing 10% FBS and 0.25 mg/ml Liberase TM
290 (Roche Life Science). Red blood cells were lysed in all samples by treatment with 1X Red Blood
291 Cell Lysis Buffer (eBioscience ThermoFisher) for 5 minutes on ice. Bone Marrow lineage-
292 negative cells were defined as negative for CD11b, Gr-1, Ter119, B220, CD3e and CD127. Bone
293 marrow HSPCs were defined as Lineage-, c-Kit+, Sca1+. Blood classical monocytes were
294 identified as CD45+, CD115^{Hi}, CD43^{Lo}, Ly6c^{Hi}; patrolling monocytes, as CD45+, CD115^{Hi},
295 CD43^{Hi}, Ly6c^{Lo}; neutrophils, as CD45+, CD115^{Int}, Ly6g+; T lymphocytes, as CD45+, CD115-,
296 B220-, CD3+; B lymphocytes, as CD45+, CD115-, CD3-, B220+; and aortic macrophages, as
297 CD45+, CD3-, Ly6g-, CD11B+, F4/80Hi. Gating strategies can be found in our previous
298 publications[17, 18]. Samples were stained with combinations of biotinylated and/or fluorescently
299 labeled antibodies in PBS with 1% FBS for 30 min on ice. The following fluorescent antibodies
300 were used for staining and flow cytometry analysis: eFluor450-conjugated anti-CD45.2, FITC-
301 conjugated anti-CD45.2, Pe-Cy7-conjugated anti-CD45.1, FITC-conjugated anti-CD11b,
302 eFluor450-conjugated anti-CD11B, PE-conjugated anti-CD115, PE-eFluor610-conjugated anti-
303 CD3, FITC-conjugated anti-CD4 (from eBioscience); APC-Cy7-conjugated anti- B220, PerCP-

304 Cy5.5-conjugated anti-Ly6G, BV510-conjugated anti-Ly6G, BV711-conjugated anti-CD43, PE-
305 Cy7-conjugated anti-c-Kit, AlexaFluor647-conjugated anti-Sca-1 (from BD Biosciences); PE-
306 conjugated anti-F4/80 (from R&D Systems); PerCP-Cy5.5-conjugated anti-CD45.1, BV510-
307 conjugated anti-CD8a, PerCP-Cy5.5-conjugated anti-mouse Ki-67 (from BioLegend).
308 Fixation/permeabilization for Ki-67 intracellular staining was achieved using commercially
309 available kits following manufacturer's instructions (Foxp3 Transcription Factor Staining Buffer
310 Set, eBioscience ThermoFisher). Dead cells were excluded from analysis by DAPI staining in
311 unfixed samples and by LIVE/DEAD Fixable Near-IR staining (ThermoFisher Scientific) in
312 fixed samples. BD LSRFortessa and BD FACSymphony Cytometers (BD Bioscience) were used
313 for data acquisition. Data were analyzed with FlowJo Software.
314
315 *Murine macrophage culture and cell cycle analysis*
316 Bone marrow-derived macrophages (BMDM) were obtained from suspensions of femoral BM
317 and differentiated for 7 days in the presence of RPMI Medium supplemented with antibiotics,
318 10% fetal bovine serum and 100 ng/ml MCSF. For cell-cycle analysis, MCSF concentration in
319 cell culture medium was decreased to 5 ng/ml for 48h to induce progressive synchronization of
320 macrophages in G0 phase (i.e. quiescence) and cell cycle re-entry was induced by treatment with
321 100 ng/ml MCSF. Macrophages were trypsinized and collected by centrifugation for 5 minutes at
322 300g. After fixation in 80% ethanol for 1 h at -20ºC, cells were incubated for at least 30 minutes
323 with 50 µg/mL propidium iodide containing 0.25 mg/mL RNAse A (both from SIGMA).
324 Labelled cells were analyzed in a BD LSRFortessa flow cytometer BD Bioscience and DNA
325 histograms were fitted into cell cycle distributions using ModFit 3.0 software (Verity Software
326 House).

327
328 *Gene expression analysis by quantitative real-time PCR (qPCR) and Western Blot.*
329
330 Total RNA from aortic arch tissue was isolated using Trizol reagent and RNeasy kits (QIAGEN).
331 RNA (1 μg) was reverse transcribed with High-Capacity cDNA Reverse Transcription Kit
332 (Applied Biosystems) and qPCR was performed with SYBR® Green PCR Master Mix (Applied
333 Biosystems) in a AB7900 Real time PCR system. Results were analyzed with the ΔΔCt method.
334 The average of 36B4 and β-actin was used as reference for normalization. Primer sequences can
335 be found in our previous publication[17]. For Western Blot analysis of protein levels, protein
336 extracts from cultured macrophages were obtained using ice-cold lysis buffer (20mM Tris-HCl
337 pH 7.5, 150 mM NaC, 1 mM NA2EDTA, 1 mM EGTA, 1% Triton) supplemented with protease
338 and phosphatase inhibitors (Roche Applied Science). Equal amounts of protein lysates were
339 resolved by SDS-PAGE and the following antibodies were used for immunoblotting: anti-p53
340 (Cell Signaling, #32532S, dil 1/1000) and HRP anti-alpha tubulin (AbCam, #ab40742, dil
341 1/2000). An ImageQuant LAS 4000 biomolecular imaging system (GE Healthcare) was used for
342 image acquisition and the ImageJ software was used for band densitometric analysis.
343
344 *Statistical analysis of data in experimental studies*
345 Data are shown as mean ± SEM unless otherwise stated. Statistical significance of differences in
346 experiments with two groups and only one variable was assessed by unpaired Student's t tests
347 (with Welch correction for unequal variance when appropriate) or Mann-Whitney U Tests.
348 Differences in experiments with more than one independent variable were evaluated by two-way
349 analysis of variance (ANOVA) with post-hoc Sidak's multiple comparison tests. All statistical
350 tests were performed using GraphPad Prism software (GraphPad Software Inc.).
351

352 **Results**

353 *Study Cohorts and Risk Of Hematologic Malignancy*

354 After excluding individuals with a known history of hematologic malignancy at enrollment, we
355 identified 37,657 unrelated individuals from the UKB and 12,465 individuals from MGBB with
356 whole exome sequencing data available for downstream analysis. Using a previously validated
357 somatic variant detection algorithm[10], we identified 2,194 (5.8%) and 657 (5.4%) CHIP carriers
358 in the UKB and MGBB, respectively (**Table III in the supplement**). Demographic and clinical
359 characteristics of these individuals, stratified by CHIP status, are depicted in **Table IV in the**
360 **supplement**. CHIP carriers tended to be older, male, previous smokers, and have a history of
361 coronary artery disease, hypertension, and hyperlipidemia (two-tailed chi-squared and Wilcoxon-
362 rank sum $P< 0.05$).

363 We first replicated known CHIP associations[10] with white blood cell (Beta 0.09 SD; 95%
364 CI 0.05-0.13; $P=1.6x10^{-5}$), monocyte (Beta 0.05 SD; 95% CI 0.01-0.09; P=0.009), neutrophil
365 (Beta 0.10 SD; 95% CI 0.06-0.14; $P=2.1x10^{-6}$), and platelet counts (Beta 0.07 SD; 95% CI 0.03-
366 0.11; P=0.0005) in UKB, with larger CHIP clone size as measured by variant allele fraction
367 (VAF) having stronger effects on blood counts (**Figure III in the supplement**). Consistent with
368 the existing literature[5, 10], CHIP also associated with incident hematologic malignancy (HR 2.20;
369 95% CI 1.70-2.85; $P=1.8x10^{-9}$) - specifically for acute myeloid leukemia (HR 8.08; 95% CI
370 4.36-14.97; $P=3.2x10^{-11}$), myeloproliferative neoplasms (HR 5.89; 95% CI 3.69-9.89; $P=9.7x10^{-}$
371 ^{14}), and polycythemia vera (HR 12.37; 95% CI 4.85-31.54; $P=1.4x10^{-7}$). This risk increased with
372 larger VAF (**Figure IV in the Supplement**).

373

374 *CHIP and Incident PAD Risk*

375 We next tested the association of CHIP status with incident PAD. Using available electronic
376 health record (EHR) data and a previously validated PAD definition[13], we identified 338 and 419
377 incident PAD cases in UKB and MGBB, respectively. CHIP associated with a 58% increased
378 risk of incident PAD in the UKB (HR_{UKB} = 1.58, 95% CI: 1.11-2.25; P=0.01, **Figure 1**), results
379 that were replicated in MGBB (Overall HR = 1.66, 95% CI: 1.31-2.11; $P=2.4x10^{-5}$). We then
380 sought to evaluate whether those with larger CHIP clone sizes (i.e., higher VAF) had greater risk
381 for PAD, as larger CHIP clones associate more strongly with adverse clinical outcomes[6]. We
382 observed a graded relationship between CHIP VAF and PAD, as those with a VAF > 10% had
383 even greater risk for an incident PAD event (Overall HR = 1.97, 95% CI: 1.44-2.71; $P=2.3x10^{-5}$,
384 **Figure 1**). Additional sensitivity analyses, including propensity score adjustment and a marginal
385 structural Cox proportional hazards model estimated through stabilized inverse-probability-
386 treatment-weight revealed similar results in the UKB (**Figure V in the supplement**). Subsequent
387 analyses showed no significant interaction between CHIP status and either age, sex, or smoking
388 status on incident PAD risk.
389
390 *CHIP and Incident Atherosclerosis Across Multiple Vascular Beds*
391 We next assessed whether CHIP was associated with 9 other incident atherosclerotic
392 diseases across multiple vascular beds. Using EHR-based disease definitions[19], we tested the
393 association of CHIP with atherosclerotic disease across the mesenteric (acute and chronic),
394 coronary, and cerebral vascular beds, as well as with aneurysmal disease (aortic and any other
395 aneurysm). We observed significant associations for coronary artery disease (HR 1.40, 95% CI:
396 1.20 to 1.63; $P=1.9x10^{-5}$), any aortic aneurysm (HR 1.74; 95% CI: 1.21 to 2.51; P=0.0028), other
397 aneurysms (HR 1.70; 95% CI: 1.23 to 2.34; P=0.0013), and chronic mesenteric ischemia (HR

398 9.12; 95% CI: 2.34 to 35.63; P=0.0015) across both cohorts, with directionally consistent effect
399 estimates observed for all the tested phenotypes (**Figure 2a**). These associations were
400 consistently stronger for large CHIP clones (**Figure VI in the supplement)**. We then created a
401 composite, incident atherosclerosis outcome combining all nine atherosclerotic phenotypes
402 ("pan-arterial atherosclerosis", **Table V in the Supplement**). CHIP associated with this
403 combined incident pan-arterial atherosclerosis endpoint (HR 1.31, 95% CI: 1.14 to 1.49,
404 $P=9.7x10^{-5}$), again with stronger effects conferred by large CHIP clones (HR 1.45; 95% CI: 1.20
405 to 1.75; P=0.00013) (**Figure 2b,c**).
406
407 *Gene-specific analyses of CHIP with incident atherosclerotic diseases*
408 Next, we sought to understand whether the clonal hematopoiesis putative driver gene
409 differentially affected the risk of acquiring atherosclerosis. Previous work has focused primarily
410 on the epigenetic regulators *DNMT3A* and *TET2*[3, 17], and whether DDR CHIP confers an
411 increased risk of atherosclerosis is unknown. We stratified the CHIP-PAD and CHIP pan-arterial
412 atherosclerosis analyses by putative driver genes and specific mutations - focusing on *DNMT3A*,
413 *TET2*, *ASXL1*, *JAK2*, the DDR genes *PPM1D* and *TP53*, and mutations that specifically disrupt
414 splicing factor genes *(LUC7L2, PRPF8, SF3B1, SRSF2, U2AF1,* and *ZRSR2)*[20]. We observed an
415 association of CHIP with PAD across the four common CHIP genes (*DNMT3A*, *TET2*, *ASXL1*,
416 and *JAK2*), with significant heterogeneity of incident PAD effect sizes across the CHIP genes
417 ($P_{heterogeneity} = 0.03$) (**Figure 3a**). This heterogeneity persisted in sensitivity analysis after
418 excluding *JAK2* carriers ($P_{heterogeneity} = 0.046$). These data also revealed the novel finding that
419 DDR *TP53* and *PPM1D* CHIP associates with incident PAD (HR 2.72; 95% CI: 1.20 to 1.75;
420 P=0.00013) and incident CAD (HR 2.51; 95% CI: 1.52-4.14; P=0.00032), with a stronger effect

421 on PAD conferred by *TP53* (HR 4.98; 95% CI: 1.23-20.09; P=0.024, **Figure 3a-c).** Similar
422 findings were observed for the incident pan-arterial atherosclerosis outcome when stratifying by
423 putative driver gene (**Figure VII in the supplement**). Further sensitivity analysis for DDR-
424 CHIP and incident PAD when excluding solid organ malignancy did not significantly change the
425 associations ($P_{heterogeneity} > 0.05$).
426
427 *Atherosclerosis development in p53-/ CHIP mice*
428 Based on our gene specific findings, we next further characterized the effects of reduced function
429 of hematopoietic p53 in atherosclerotic mice. To mimic CHIP and test whether the expansion of
430 p53-deficient hematopoietic cells contributes to atherosclerosis, a competitive bone marrow
431 transplantation (BMT) strategy was used to generate atherosclerosis-prone *Ldlr*-/- chimeric mice
432 carrying 20% *Trp53*-/- hematopoietic cells (20% KO-BMT mice). These mice then consumed a
433 high fat/high cholesterol diet for 9 weeks to induce atherosclerosis development. To distinguish
434 donor *Trp53*-/- and *Trp53*+/+ cells in this experimental setting, *Trp53*+/+ cells were obtained
435 from mice carrying the CD45.1 variant of the CD45 hematopoietic antigen, whereas *Trp53*-/-
436 cells were obtained from mice carrying the CD45.2 variant of this protein. Control mice (20%
437 WT-BMT) were transplanted with 20% CD45.2+ *Trp53*+/+ cells and 80% CD45.1+ *Trp53*+/+
438 cells (**Figure 4a and Figure II in the supplement**). Flow cytometry analysis of CD45.2+ blood
439 cells established that this BMT strategy led to a modest, but significant expansion of donor
440 *Trp53*-/- BM-derived cells compared to *Trp53*+/+ cells in both BM hematopoietic
441 stem/progenitor cells (HSPCs) and circulating white blood cells (**Figure 4B,C**), consistent with
442 previous studies[21-23]. Transplanted *Trp53*-/- BM cells expanded into all blood cell lineages to a
443 similar extent, but this relative expansion did not affect absolute blood cell counts (**Figure VIII**

444 **in the supplement**). Having validated this mouse model of p53 CHIP based on a competitive
445 BMT strategy, we next assessed whether this phenomenon affects the development of
446 atherosclerosis or related metabolic abnormalities. The presence and expansion of *Trp53*-/- cells
447 led to a significant ~40% increase in plaque size in the aortic root of male *Ldlr*-/- mice (**Figure**
448 **4D**), without affecting body weight, spleen weight or serum cholesterol levels (**Figure VIII in**
449 **the supplement, C-E**). Similar results were obtained in female *Ldlr*-/- mice (**Figure IX in the**
450 **supplement**). In contrast to previous work on *DNMT3A/TET2* CHIP, the expansion of p53-
451 deficient cells[12, 17, 18, 24, 25] did not affect the expression of the pro-inflammatory cytokines IL-6
452 and IL-1β in the atherosclerotic aortic wall (**Figure X in the supplement**).
453
454 *Proliferation and expansion of p53-deficient macrophages in the murine atherosclerotic aorta*
455 Increased atherogenesis in mice carrying *Trp53*-/- cells was paralleled by a substantial increase
456 in plaque macrophage content, as assessed by immunohistological staining of Mac2, with no
457 significant changes in other cell components (**Figure 5A**), suggesting a contribution of increased
458 arterial macrophage burden to accelerated atherosclerosis in conditions of p53 CHIP. Flow
459 cytometry analysis of matched samples from blood and digested atherosclerotic aortae from
460 20% KO-BMT mice revealed substantially higher chimerism in aortic macrophages (~76%
461 *Trp53*-/-) than in blood classical monocytes (~48%), the major source of plaque macrophages
462 (**Figure 5B**). This expansion of p53-deficient macrophages within the vascular wall was
463 paralleled by a 2-fold increase in the frequency of proliferating cells within the CD45.2+ *Trp53*-
464 /- aortic macrophage population compared to CD45.2+ *Trp53*+/+ macrophages, as assessed by
465 flow cytometry analysis of the proliferation-related antigen Ki-67 (**Figure 5C).** Consistent with
466 our observations *in vivo*, cultured *Trp53*-/- macrophages exhibit accelerated mitotic cell cycle

467 progression, with a >2-fold increase in the percentage of S-phase cells upon stimulation with
468 macrophage colony stimulating factor (MCSF), a major determinant of plaque macrophage
469 proliferation[26] (**Figure 5D**). *Trp53* expression analysis suggests a central role of p53 in the
470 normal regulation of macrophage cell cycle progression, as p53 was expressed in quiescent
471 macrophages at the transcript and protein level and further induced after MCSF stimulation
472 (**Figure 5E,F**). Furthermore, p53-deficient macrophages exhibited major changes in the
473 expression of pivotal regulators of cell cycle entry and progression, such as *Cdkn1a*/p21^{Cip1} and
474 Cyclin B1 (**Figure 5G**).
475

476 **Discussion**

477 This study combined exome sequencing data across two biobanks to detect somatic
478 mutations in over 50,000 individuals and observed that the presence of CHIP was significantly
479 associated with an increased risk of developing PAD and atherosclerosis across multiple arterial
480 beds. Increased risk was differentially observed across CHIP driver genes with evidence of a
481 graded relationship with CHIP VAF, with large CHIP clones conferring greater risk of disease.
482 Lastly, analysis of p53 CHIP using a BMT murine model showed increased aortic atherosclerotic
483 plaque among p53 CHIP carriers accompanied by expansion of plaque macrophages, supporting
484 a direct contribution of p53-mutant hematopoietic cells to accelerated atherogenesis.

485 These findings permit several conclusions. First, in humans, CHIP appears to promote
486 atherosclerosis across the entire arterial system. Previous work linked CHIP with increased risk
487 of coronary artery disease and early-onset MI[2, 3]. We build on these findings by demonstrating
488 that CHIP is also associated with PAD, and a composite pan-arterial atherosclerosis outcome
489 reflective of an increased burden of atherosclerosis throughout the human arterial system. In

490 addition, we observed suggestive CHIP associations with aneurysmal degeneration of the aorta.
491 The genetic and epidemiologic risk factors underlying atherosclerotic occlusive disease and
492 AAA overlap considerably[27], and substantial evidence implicates inflammation and macrophage
493 infiltration in driving this aortic disease[28]. The observed link between CHIP and aneurysmal
494 disease warrants further investigation in future studies.

495 Second, DDR gene CHIP appears to confer an increased risk of atherosclerotic
496 cardiovascular disease. In previous work, Jaiswal et al demonstrated an increased risk of
497 coronary artery disease among individuals with CHIP through *DNMT3A, TET2, ASXL1,* and
498 *JAK2* somatic driver mutations[3]. DDR CHIP is often observed among individuals following
499 cytotoxic chemotherapy for the treatment of malignancy and has been linked to the development
500 of therapy-related myeloid neoplasms, but limited evidence is available to inform clinical
501 decision making regarding whether DDR CHIP carriers have increased risk of cardiovascular
502 disease. The current study demonstrates that CHIP related to DDR-genes (*TP53, PPM1D*)
503 confers an increased risk of developing atherosclerosis. These findings lend human genetic
504 support to the concept that post-cytotoxic chemotherapy patients may benefit from surveillance
505 for atherosclerotic conditions in addition to therapy-related myeloid neoplasms.

506 Third, CHIP related to *TP53* mutations appears to drive atherosclerosis risk via expansion
507 of p53-deficient macrophages in occlusive plaque lesions. Previous experimental studies
508 assessed the role of p53 in atherogenesis using mice engineered to exhibit gain or loss of
509 function of p53 in the whole body or in specific cell types, with a variety of results[29-35]. Here we
510 demonstrate that carrying a fraction of p53-deficient blood cells is sufficient to accelerate
511 atherosclerosis development, as these cells have a selective advantage to expand, both in HSPCs
512 within the BM and in macrophages within the arterial wall, leading to increased macrophage

513 burden in the atherosclerotic plaque. Mechanistically, p53-deficient macrophage expansion
514 seems related to increased proliferation, a major driver of macrophage burden in atherosclerotic
515 plaques[36]. Although p53 expression is typically induced by DNA damage or other kinds of
516 cellular stress, we found that it is expressed in resting conditions in cultured macrophages and
517 further induced by mitogenic stimulation, suggesting a physiological role in the regulation of
518 macrophage cell cycle progression. Accordingly, p53-deficient macrophages exhibited
519 accelerated cell cycle kinetics. Overall, these experimental findings provide support to the notion
520 that *TP53* CHIP mutations contribute directly to accelerated atherosclerosis and highlight major
521 differences in the mechanisms underlying accelerated atherosclerosis in CHIP driven by
522 mutations in *TP53* or epigenetic regulators. Previous murine studies on *Tet2* CHIP showed that
523 TET2-deficient cells expand in bone marrow and blood, but not in the atherosclerotic plaque. In
524 contrast, we found that p53 exhibits a double competitive advantage, expanding in both the BM
525 and arterial wall, which suggests that small *TP53*-mutant blood clones may be sufficient to
526 accelerate atherosclerosis development. Evaluating this possibility will require additional studies
527 using high sensitivity sequencing strategies. Furthermore, in contrast to previous reports related
528 to *DNMT3A/TET2* CHIP[12, 17, 18, 24, 25], we did not observe a significant effect of p53 deficiency on
529 the expression of the pro-inflammatory cytokines IL-1β and IL-6. These results are consistent
530 with previous human data showing that circulating levels of pro-inflammatory cytokines are
531 significantly increased in carriers of CHIP driven by mutations in these epigenetic regulators, but
532 not in carriers of mutations in *TP53* or *PPM1D*[10]. These mechanistic differences between *TP53*-
533 CHIP and *DNMT3A/TET2*-CHIP require consideration when designing preventive care strategies
534 targeting the effects of CHIP on atherosclerosis. Thus, while the pathogenic effects of TET2-
535 CHIP may be prevented by targeting IL-1β-driven inflammation[17], accelerated atherosclerosis

536 associated with *TP53* mutations may be better tackled by other strategies. Additional
537 experimental and clinical studies should evaluate these opportunities for personalized medicine
538 in the context of CHIP.

539 Lastly, a recent publication has generated a novel hypothesis regarding the relationship
540 between CHIP and atherosclerosis[37]. In their analysis, Heyde et al. suggest that CHIP may be a
541 symptom of the atherosclerosis trait complex (the interplay of chronic inflammation,
542 hyperlipidemia, and arterial plaque), rather than a causal risk factor, based on murine and human
543 observations that atherosclerosis may accelerate HSC proliferation and somatic evolution. While
544 their study engenders an intriguing hypothesis, there are several observations in the literature and
545 in our current study that we believe do not support this interpretation. Firstly, in the Heyde et al.
546 study, *Ldlr*-null mice irradiated and transplanted with bone marrow of *Tet2* -/- mice that were fed
547 an atherogenic diet demonstrated greater *Tet2* -/- neutrophil and monocyte expansion than
548 similar mice fed normal chow. However, in marked contrast, we previously showed that *Tet2*-/-
549 cells expand similarly when *Ldlr*-null mice are fed either a high cholesterol diet or normal
550 chow[17]. Furthermore, in our prior work, the expansion of *Tet2*-/- cells was completely unaffected
551 by treatment with a pharmacological NLRP3 inhibitor, even though this inhibitor led to a 2-fold
552 decrease in atherosclerotic plaque size[17]. Secondly, in our current analysis of the pan-arterial
553 atherosclerosis endpoint, CHIP was associated with incident atherosclerotic events among a pool
554 of individuals without any history of atherosclerosis at baseline - suggesting that CHIP precedes
555 clinically significant occlusive disease. Thirdly, Heyde et al. state that the uniform hazard ratios
556 observed for the CHIP-coronary artery disease association provide supportive evidence for the
557 notion that atherosclerotic disease precedes the development of clonal hematopoiesis. However,
558 in our study we identify significant heterogeneity of incident PAD effect sizes when stratifying

559 by CHIP genes, as well as a dose-response relationship between CHIP clone size (or VAF) and
560 incidence of atherosclerosis, suggesting that CHIP genes vary in their effect on incident PAD
561 risk, and that expanded CHIP variants have a stronger influence on future atherosclerotic risk.
562 Thus, given the 1) association with incident atherosclerotic disease, 2) dose-response relationship
563 with CHIP clone size and heterogeneity by CHIP gene, and 3) that *TP53*, *TET2*, and *JAK2*[38]
564 appear to drive atherosclerosis through disparate mechanisms, clonal hematopoiesis acting as a
565 causal risk factor appears to be a more parsimonious explanation to unify these findings.

566 Several limitations merit mention. First, our PAD and cardiovascular disease phenotypes
567 are based on EHR data and may result in misclassification of case status. Such misclassification
568 would likely reduce statistical power for discovery and on average bias results toward the null.
569 Second, selection bias from differential loss-of-follow up, volunteer bias, and missingness in
570 covariates may be present given the nature of the genetic biobanks used in this study. Third,
571 while we maximized the number of participants in our analysis of CHIP and additional
572 atherosclerotic diseases, it may still have been underpowered for certain phenotypes. Lastly, the
573 cohorts in these studies are largely of European ancestry; while prior reports have not observed
574 significant phenotypic differences in CHIP associations by ancestry[5, 12], further epidemiological
575 studies in ethnically diverse individuals are required to ensure that this is the case for PAD as
576 well.

577 In conclusion, CHIP is associated with incident atherosclerosis in multiple vascular beds,
578 with murine evidence of increased plaque among *TP53* CHIP carriers through an expansion of
579 plaque macrophages (**Figure 6**). The observations presented here expand insight into CHIP-
580 mediated atherosclerosis. The novel finding that DDR gene CHIP plays a particular role in PAD
581 raises new questions regarding the mechanisms of regional heterogeneity of atherosclerotic

582 involvement in face of systemic exposure to traditional risk factors such as dyslipidemia,

583 hypertension, and smoking.

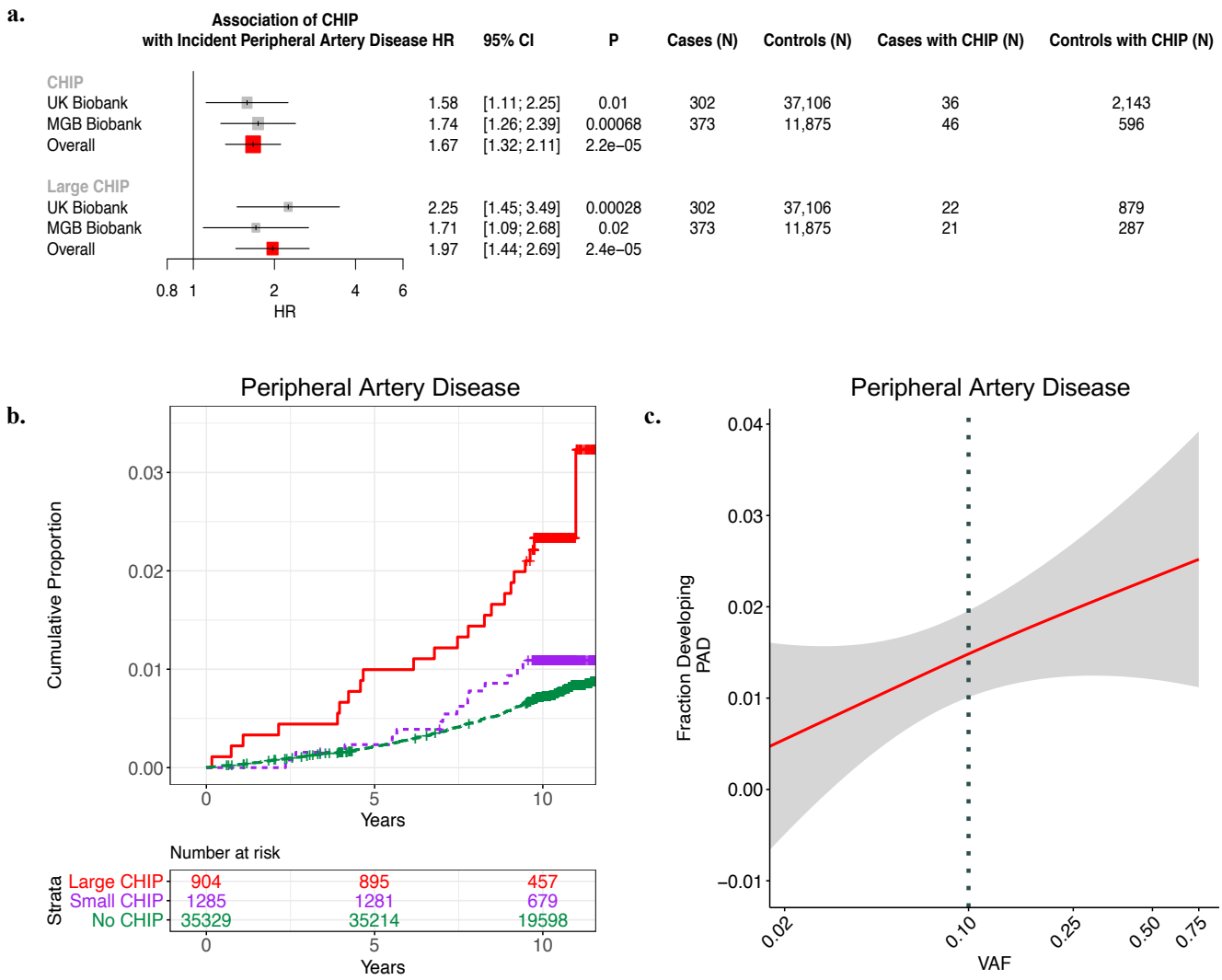

Figure 1. CHIP and incident PAD risk. a) Association of CHIP and large CHIP (VAF>10%) carrier state with incident PAD events in the UK Biobank (UKB) and Mass General Brigham Biobank (MGBB). Results were combined using an inverse-variance weighted fixed effects meta-analysis. b) Cumulative proportion of individuals developing PAD stratified by CHIP VAF clone size category in the UK Biobank. c) Fraction of individuals developing incident PAD by CHIP VAF in the UK Biobank. CHIP = clonal hematopoiesis of indeterminate potential; VAF = variant allele fraction; PAD = peripheral artery disease

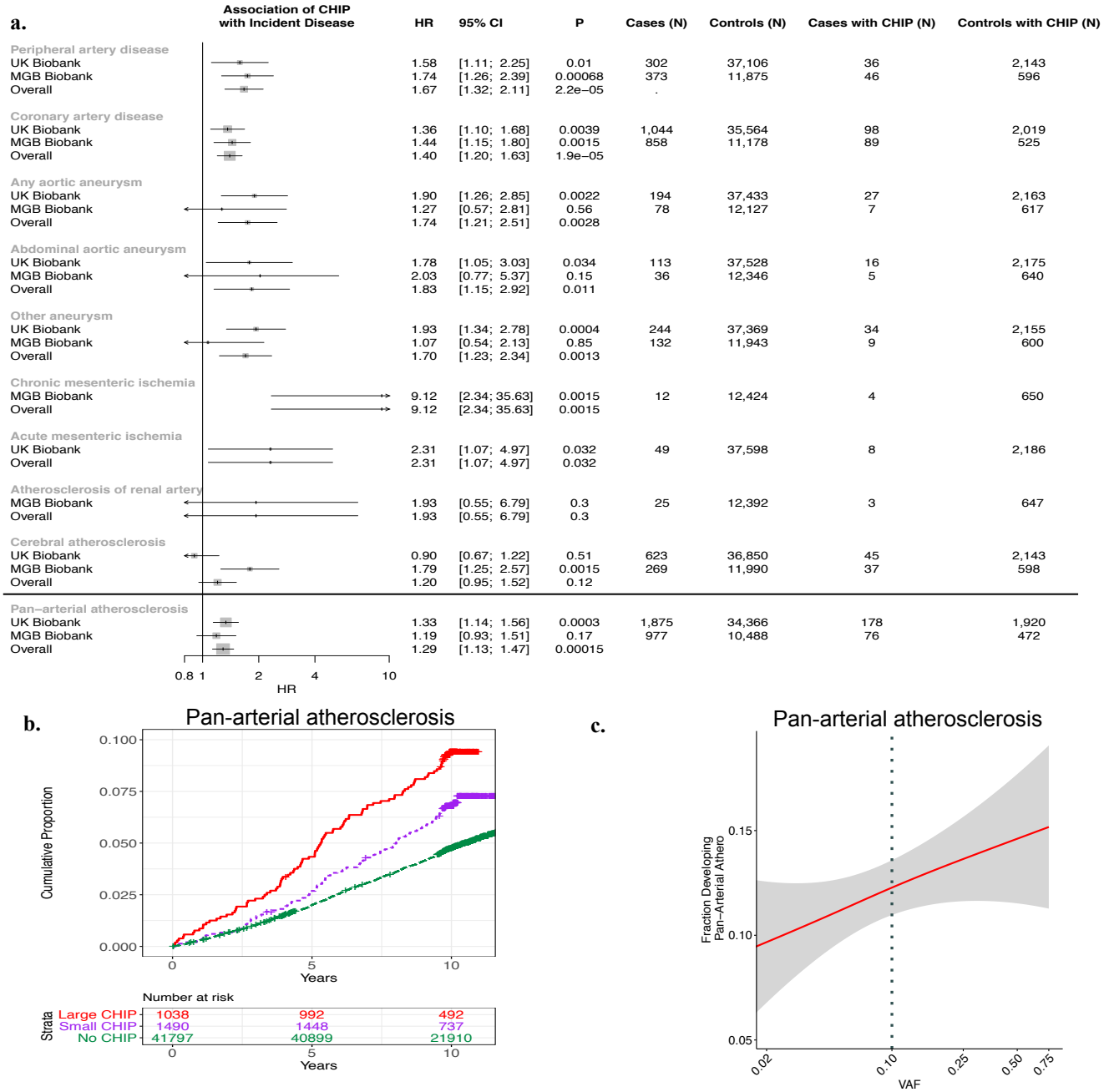

Figure 2. CHIP and incident pan-arterial atherosclerosis risk. a) Association of CHIP with 9 incident atherosclerotic diseases separately and combined in a 'Pan-arterial atherosclerosis' phenotype in the UKB, MGBB, and meta-analyzed across both studies ("Overall"). b) Cumulative risk of incident atherosclerosis across the composite 'pan-arterial atherosclerosis' phenotype stratified by no CHIP, small CHIP (VAF<10%), and large CHIP (VAF≥10%) carrier state in the UK Biobank. c) Association of CHIP VAF with fraction of individuals developing pan-arterial atherosclerosis in the UK Biobank. CHIP = clonal hematopoiesis of indeterminate potential; VAF = variant allele fraction; PAD = peripheral artery disease

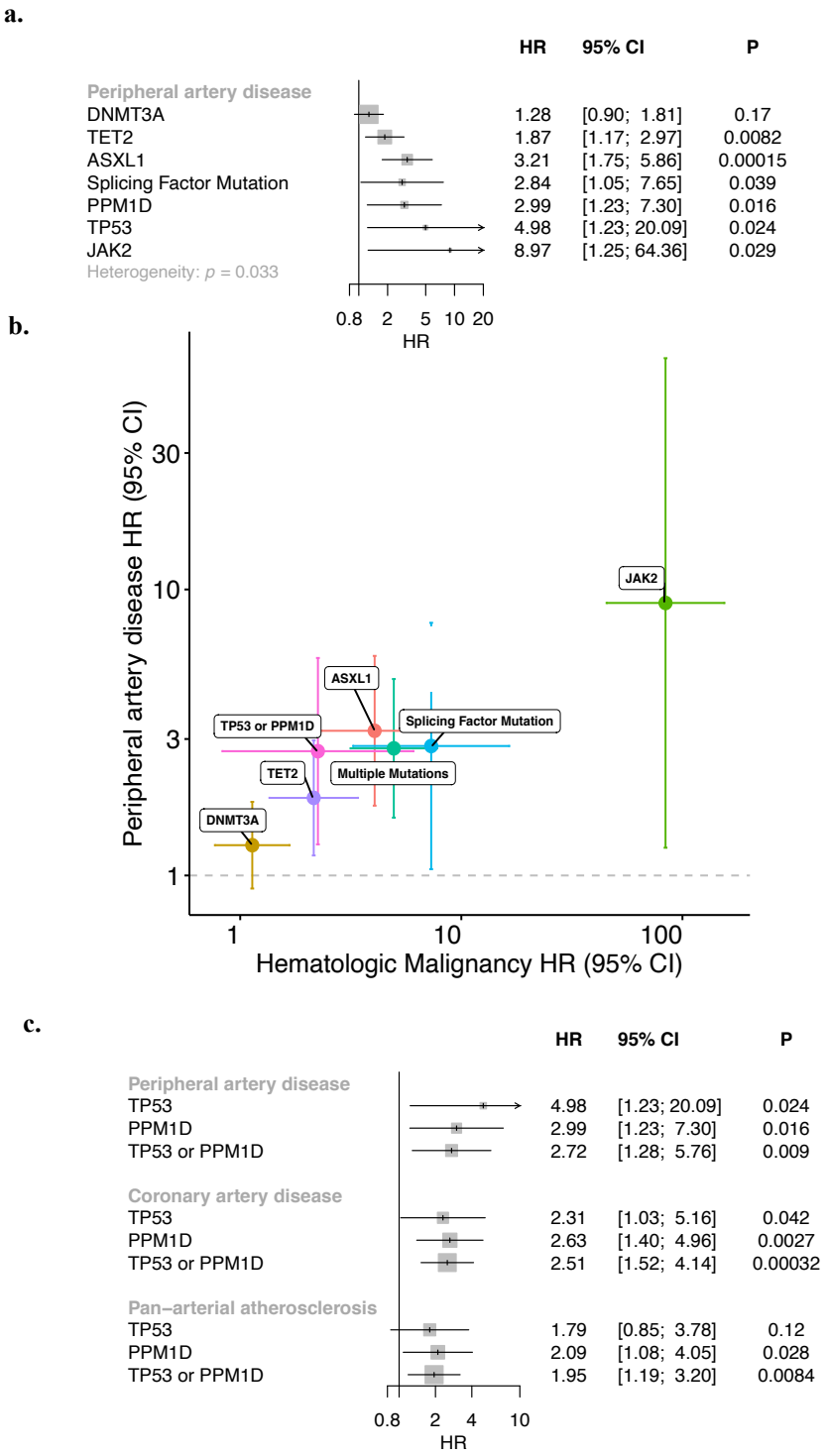

Figure 3: Gene-specific association of CHIP with incident peripheral artery disease (PAD). a) CHIP-PAD association analyses stratified by putative CHIP driver gene. Results following meta-analysis across the UKB and MGBB are shown. b) Gene-specific comparison of HR and 95% CI for hematologic malignancy (x-axis) and PAD (y-axis) in the UKB. c) Association of DDR CHIP (*PPM1D or TP53*) with incident peripheral artery disease, coronary artery disease, and pan-vascular atherosclerosis. Results across UK Biobank and MGB Biobank were combined using an inverse-variance weighted fixed effects meta-analysis. CHIP = clonal hematopoiesis of indeterminate potential; DDR = DNA-damage repair; VAF = variant allele fraction; PAD = peripheral artery disease

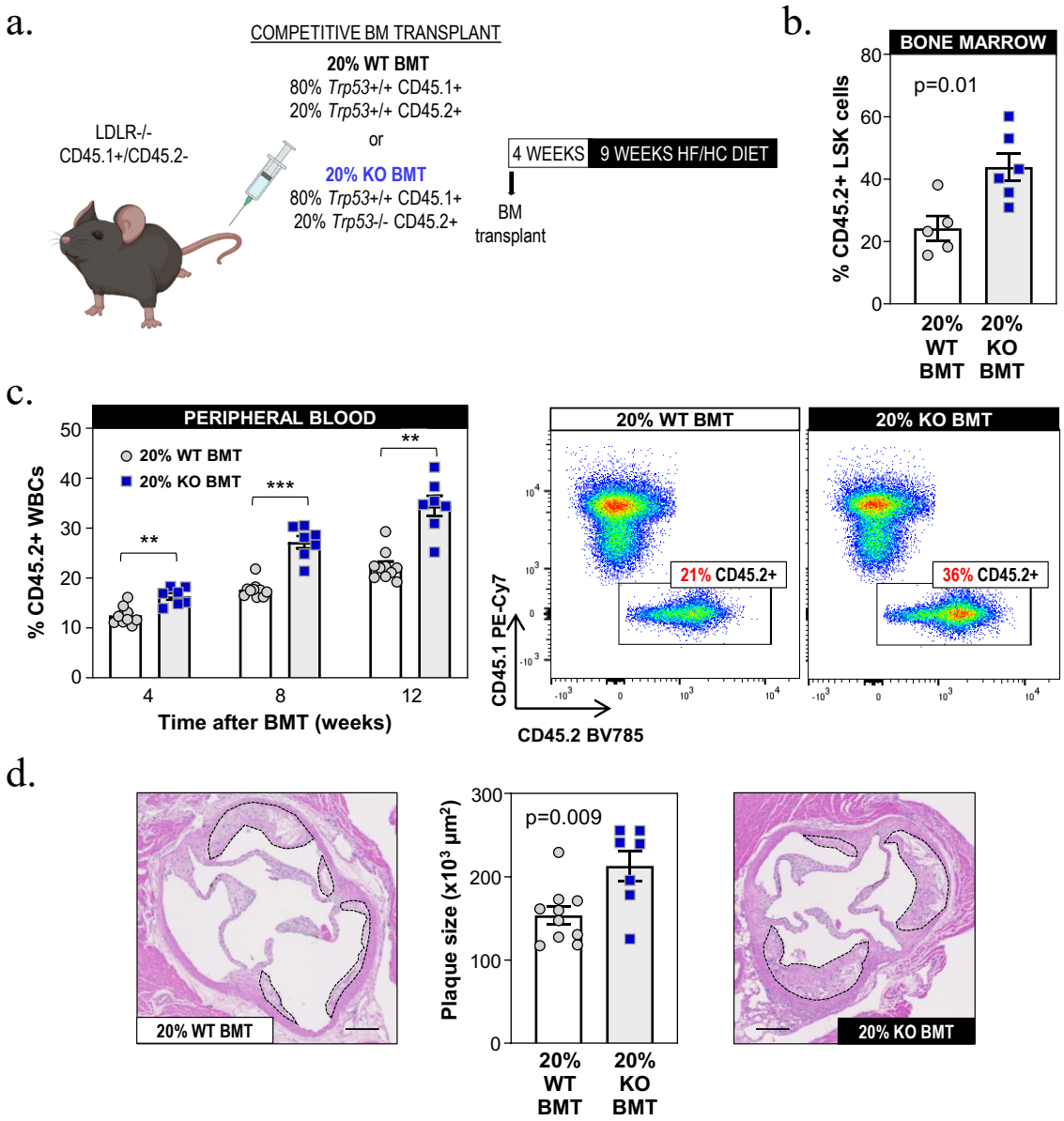

Figure 4: Accelerated atherosclerosis in a murine model of *TP53* mutation-driven CHIP. a) Summary of the competitive BMT approach and the timeline of these studies. 20% KO-BMT male mice and 20% WT-BMT controls were fed a high-fat/high-cholesterol (HF/HC) diet for 9 weeks, starting 4 weeks after BMT (n=10 20% WT-BMT, n=7 20% KO-BMT, unless otherwise noted). b) Percentage of CD45.2+ cells in the bone marrow HSPC population (Lin- Sca1+ cKit+ cells) after 9 weeks on HF/HC diet (13 weeks post-BMT), evaluated by flow cytometry (n= 5 20% WT-BMT, n=6 20% KO-BMT). c) Percentage of CD45.2+ in white blood cells, evaluated by flow cytometry (**p<0.01, ***p<0.001). Representative CD45.1/CD45.2 dot plots are shown. d) Aortic root plaque size. Representative images of hematoxylin and eosin-stained sections are shown; atherosclerotic plaques are delineated by dashed lines. Scale bars, 100 µm.

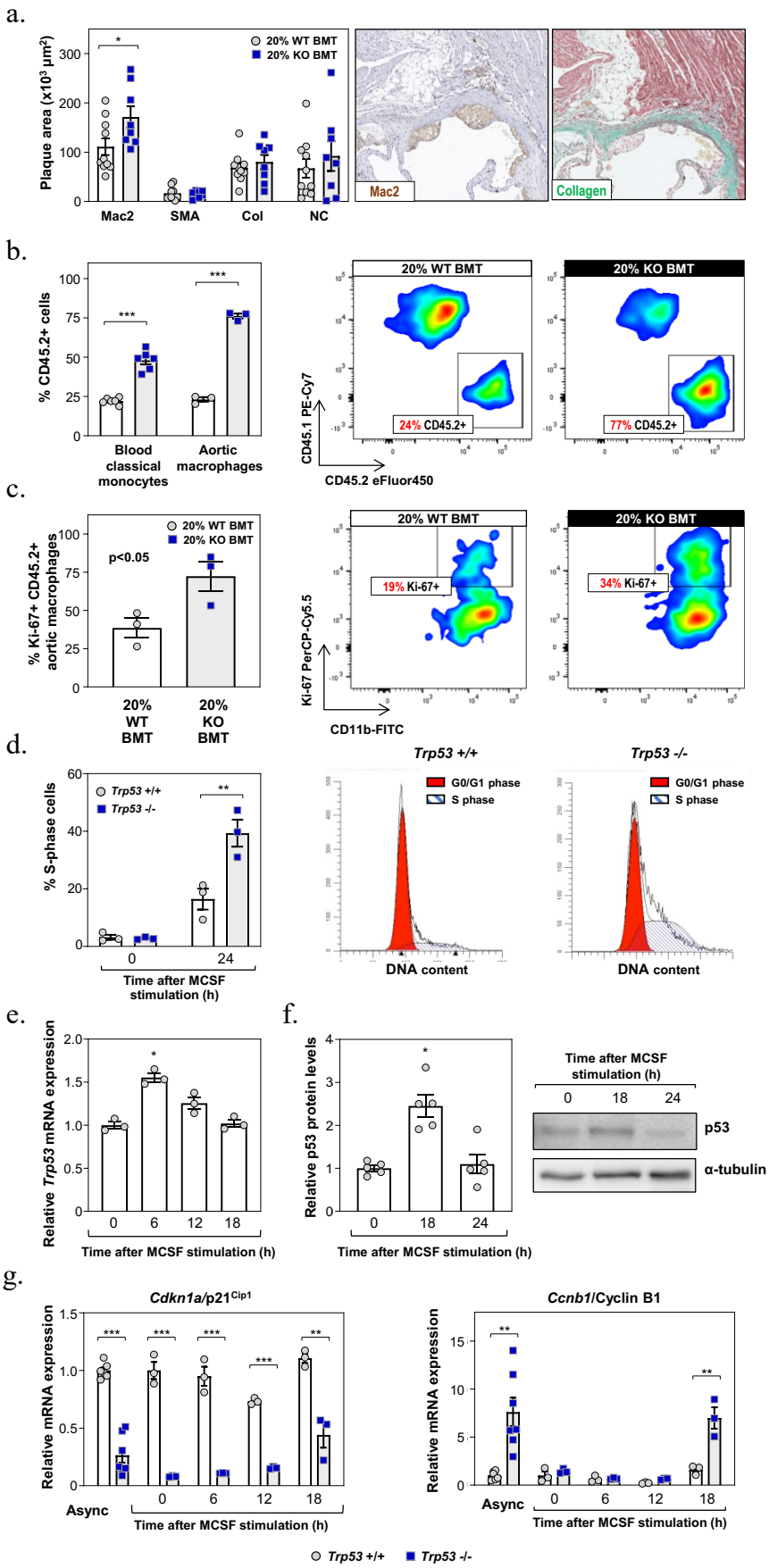
a.
Plaque area (x10³ µm²)
20% WT BMT
20% KO BMT
Mac2
SMA
Col
NC
Mac2
Collagen
b.
% CD45.2+ cells
Blood classical monocytes
Aortic macrophages
20% WT BMT
20% KO BMT
24% CD45.2+
77% CD45.2+
CD45.1 PE-Cy7
CD45.2 eFluor450
c.
% Ki-67+ CD45.2+ aortic macrophages
p<0.05
20% WT BMT
20% KO BMT
19% Ki-67+
34% Ki-67+
Ki-67 PerCP-Cy5.5
CD11b-FITC
d.
% S-phase cells
Trp53 +/+
Trp53 -/-
Time after MCSF stimulation (h)
G0/G1 phase
S phase
DNA content
e.
Relative Trp53 mRNA expression
Time after MCSF stimulation (h)
f.
Relative p53 protein levels
Time after MCSF stimulation (h)
p53
α-tubulin
g.
Cdkn1a/p21Cip1
Ccnb1/Cyclin B1
Relative mRNA expression
Async
Time after MCSF stimulation (h)
Trp53 +/+
Trp53 -/-

685

686 **Figure 5: Increased proliferation and expansion of p53-deficient macrophages.** a) Plaque
687 composition in 20% KO BMT female mice (n=10) and controls (n=8) quantified as absolute
688 intimal content of macrophages (Mac2 antigen immunostaining), vascular smooth muscle cells
689 (smooth muscle α-actin, SMA immunostaining), collagen (Masson's trichrome staining) and
690 necrotic core (collagen-free acellular regions). Representative images of Mac2- and collagen-
691 stained histological sections of 20% KO BMT mice are shown. b) Percentage of CD45.2+ cells
692 within the aortic macrophage population (CD3-, Ly6g-, CD11B+, F4/80^{Hi}, n = 3 pools of two
693 aortic arches per BM genotype) and blood classical monocytes (CD3-, CD115^{Hi}, Ly6g-, CD43^{Lo},
694 Ly6c^{Hi}, n=6 per BM genotype) of 20% KO BMT mice and controls, evaluated by flow
695 cytometry. Representative CD45.1/CD45.2 plots of aortic macrophages are shown. c) Percentage
696 of Ki-67+ proliferating cells within the aortic CD45.2+ macrophage population of 20% KO
697 BMT mice and controls (n = 3 pools of two aortic arches per BM genotype), evaluated by flow
698 cytometry. Representative plots are shown. d) % of S-phase cells in cultures of *Trp53*-/- and +/+
699 murine bone marrow-derived macrophages, evaluated by propidium iodide staining of cellular
700 DNA content and flow cytometry; treatment with MCSF was used to induce cell cycle entry and
701 progression in quiescent G0-synchronized macrophages (a representative experiment with
702 macrophages from n=3 mice per genotype is shown). e, f) qPCR (e) and Western Blot (f)
703 analyses of *Trp53* expression in cultured macrophages after MCSF mitogenic stimulation. p53
704 protein levels were normalized to α-tubulin. A representative blot is shown. g) Expression of cell
705 cycle regulators *Cdkn1a*/p21^{Cip1} and *Ccnb1*/Cyclin B1 in cultured *Trp53*-/- and +/+ macrophages
706 proliferating asynchronously (Async) or after MCSF stimulation. *$p<0.05$, **$p<0.01$,
707 ***$p<0.001$.

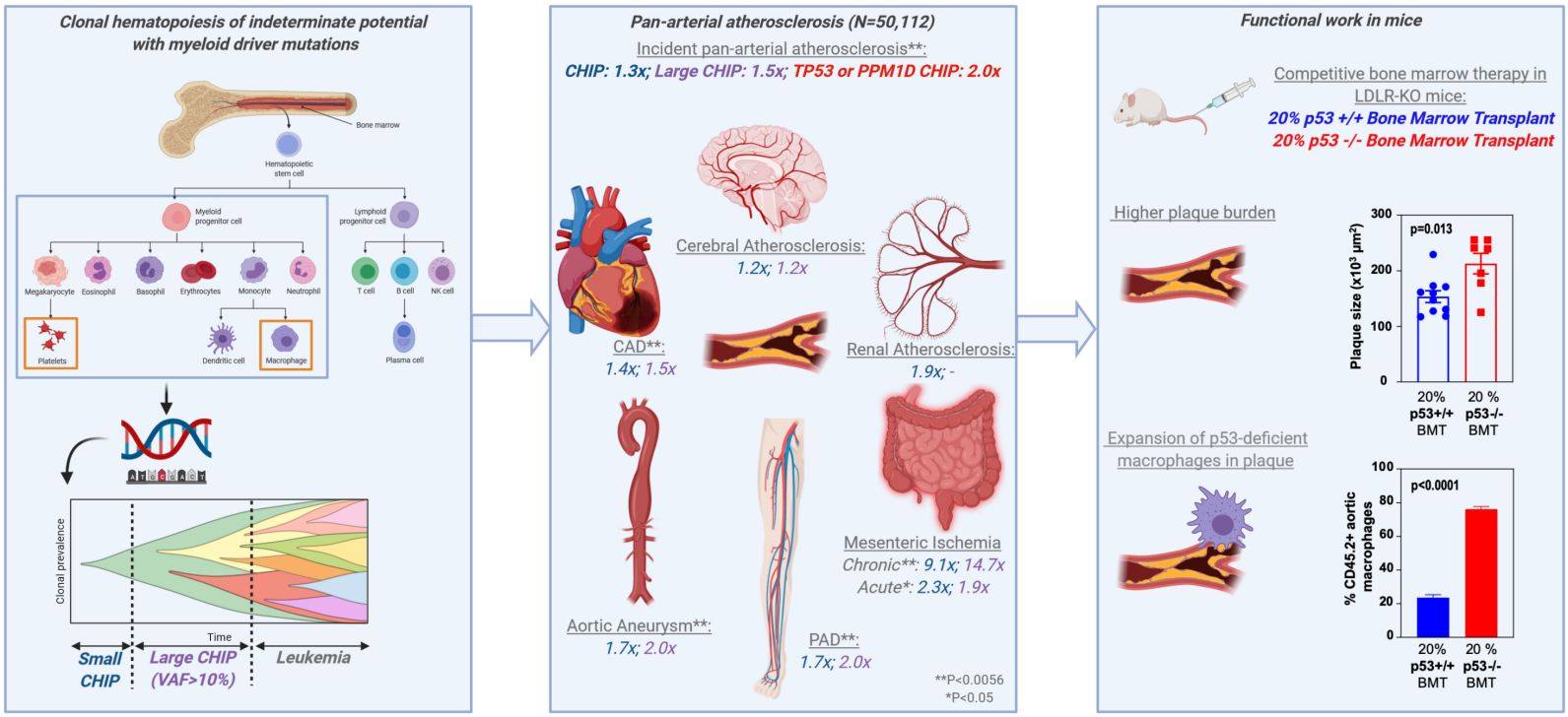

Figure 6. In this study, we assessed the association of clonal hematopoiesis of indeterminate potential (CHIP) with myeloid driver mutations with pan-arterial atherosclerosis. CHIP is a category of age-related somatic variants which are associated with incident leukemia and thought to be implicated in atherosclerosis primarily by altering macrophage function and promoting thrombosis. CHIP clones can be characterized by the fraction of blood cells carrying the clone, referred to as the variant allele fraction (VAF); here we categorized large CHIP clones as variants with VAF>10%. Across 50,112 individuals from the UK Biobank and Mass-General Brigham Biobank, we observed that CHIP is associated with increased risk of incident peripheral and pan-arterial atherosclerosis, with stronger effects conferred by large CHIP clones (HR 1.5x). In addition, we observed and a novel associations for *TP53* and *PPM1D* CHIP (HR 2.0x). CHIP was found to be individually associated with a variety of atherosclerotic conditions, with Bonferroni-significant associations (double-starred, **) identified for peripheral artery disease (PAD), coronary artery disease (CAD), aortic aneurysm, and chronic mesenteric ischemia. HR for CHIP are displayed in blue and for large CHIP in purple. Functional analysis was performed to further investigate the observed TP53-PAD association. *Ldlr*-KO 20% p53 -/- bone-marrow transplanted mice had a significant increase in plaque size, with significant expansion of p53-deficient macrophages in plaque (P<0.001) at 12 weeks.

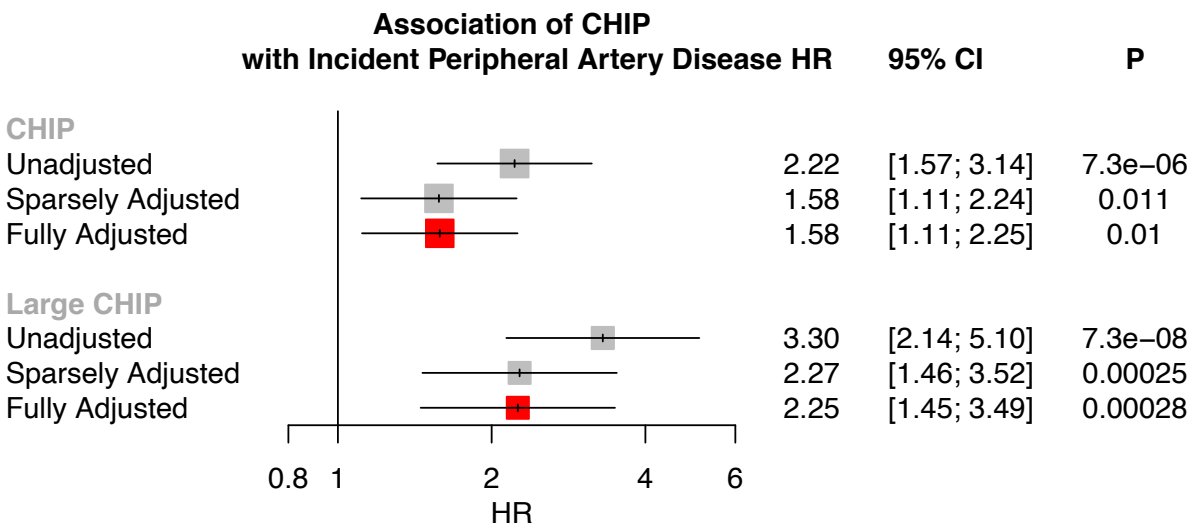

Supplementary Figure I. Association of CHIP and Large CHIP (variant allele fraction>10%) with PAD in the UKB under 1) unadjusted, 2) sparsely adjusted, and 3) fully adjusted models, where sparsely adjusted refers to the following covariates: age, age^2, sex, smoking status, Townsend deprivation index, and the first ten principal components of genetic ancestry, and the fully adjusted model additionally includes normalized BMI, prevalent hypertension, hyperlipidemia, and type 2 diabetes as covariates. Given the minimal difference between the sparsely adjusted and fully adjusted model, the sparsely adjusted model was moved forward for use in analysis.

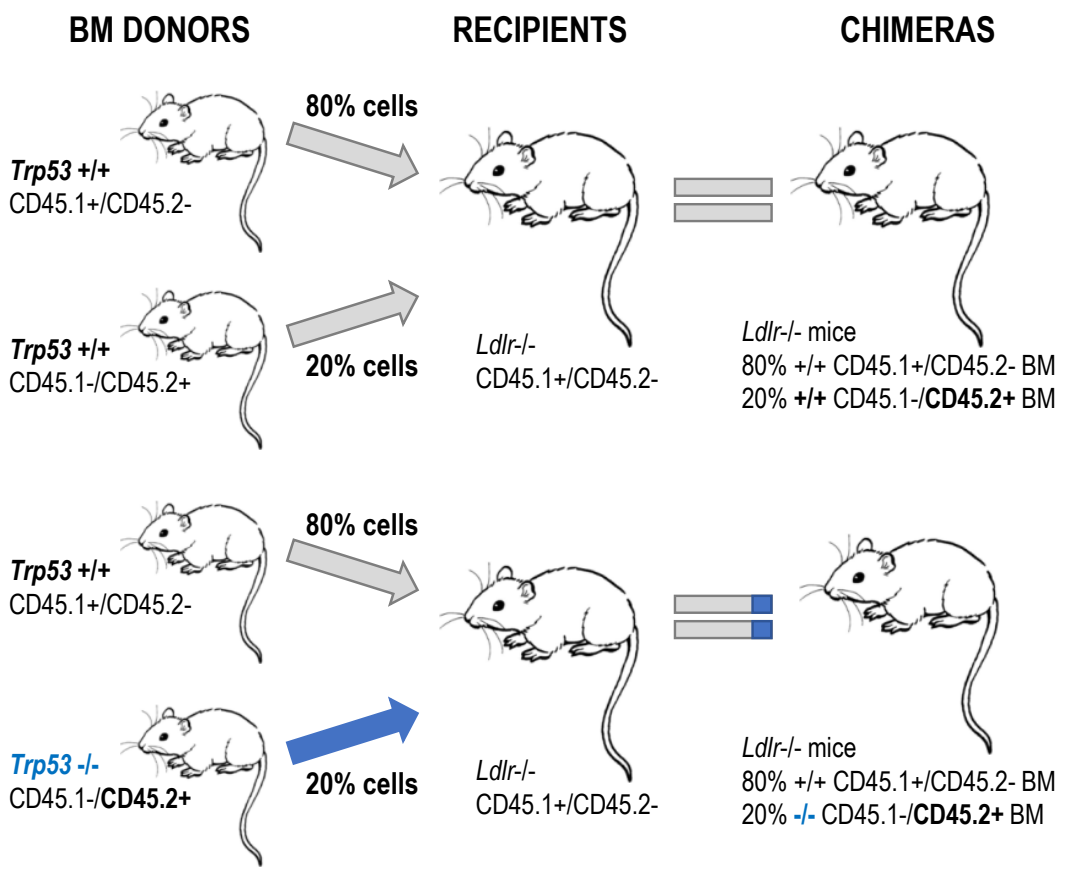

Supplementary Figure II. Competitive bone marrow transplantation approach to generate a murine model of p53 CHIP

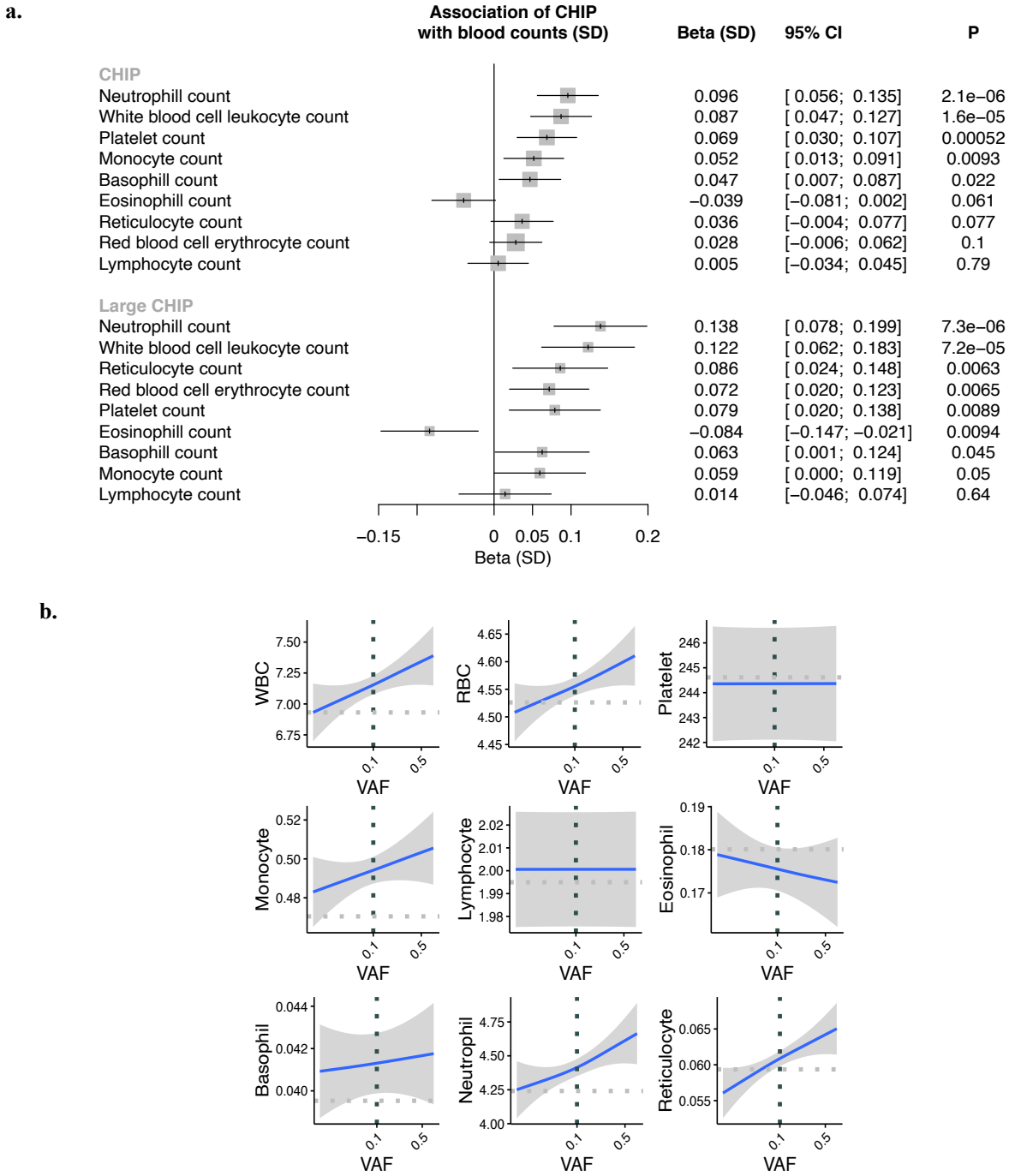

Supplementary Figure III. Association of CHIP with blood counts among individuals without prevalent hematologic malignancy in the UK Biobank. Blood counts were acquired at time of blood draw for whole exome sequencing. a) Association of CHIP and Large CHIP with normalized blood counts (SD). Associations are adjusted for age, age^2, sex, smoking status, and the first ten principal components of genetic ancestry. b) Association of CHIP variant allele frequency (VAF) with blood counts (in units of 10^9 cells/L). The gray horizontal dotted lines reflect average counts across non-CHIP carriers. The vertical black dotted line reflects the cutoff VAF for Large CHIP (VAF>0.1). CHIP = clonal hematopoiesis of indeterminate potential; VAF = variant allele fraction

a.

Association of CHIP with Incident Disease	HR	95% CI	P	Cases (N)	Controls (N)	Cases with CHIP (N)	Controls with CHIP (N)
CHIP							
Hematologic Malignancy	2.20	[1.70; 2.85]	1.8e−09	478	37,179	69	2,125
Myeloproliferative Neoplasm	5.89	[3.69; 9.39]	9.7e−14	84	37,573	27	2,167
Acute Myeloid Leukemia	8.08	[4.36; 14.97]	3.2e−11	45	37,612	17	2,177
Polycythemia Vera	12.37	[4.85; 31.54]	1.4e−07	19	37,638	8	2,186
Large CHIP							
Hematologic Malignancy	3.45	[2.54; 4.70]	3e−15	478	37,179	46	865
Myeloproliferative Neoplasm	10.62	[6.37; 17.72]	1.4e−19	84	37,573	21	890
Acute Myeloid Leukemia	9.86	[4.58; 21.24]	5e−09	45	37,612	9	902
Polycythemia Vera	22.84	[8.19; 63.72]	2.3e−09	19	37,638	6	905

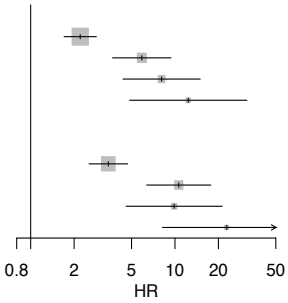

b

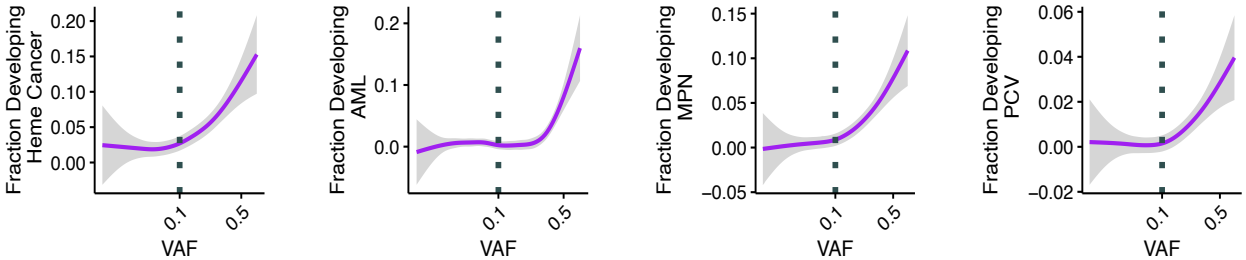

Supplementary Figure IV: Association of CHIP (a) and VAF (b) with incident hematologic malignancy among individuals without prevalent hematological malignancy in the UK Biobank. Associations are adjusted for age, age^2, sex, smoking status, Townsend deprivation index, and the first ten principal components of genetic ancestry. CHIP = clonal hematopoiesis of indeterminate potential; VAF = variant allele fraction

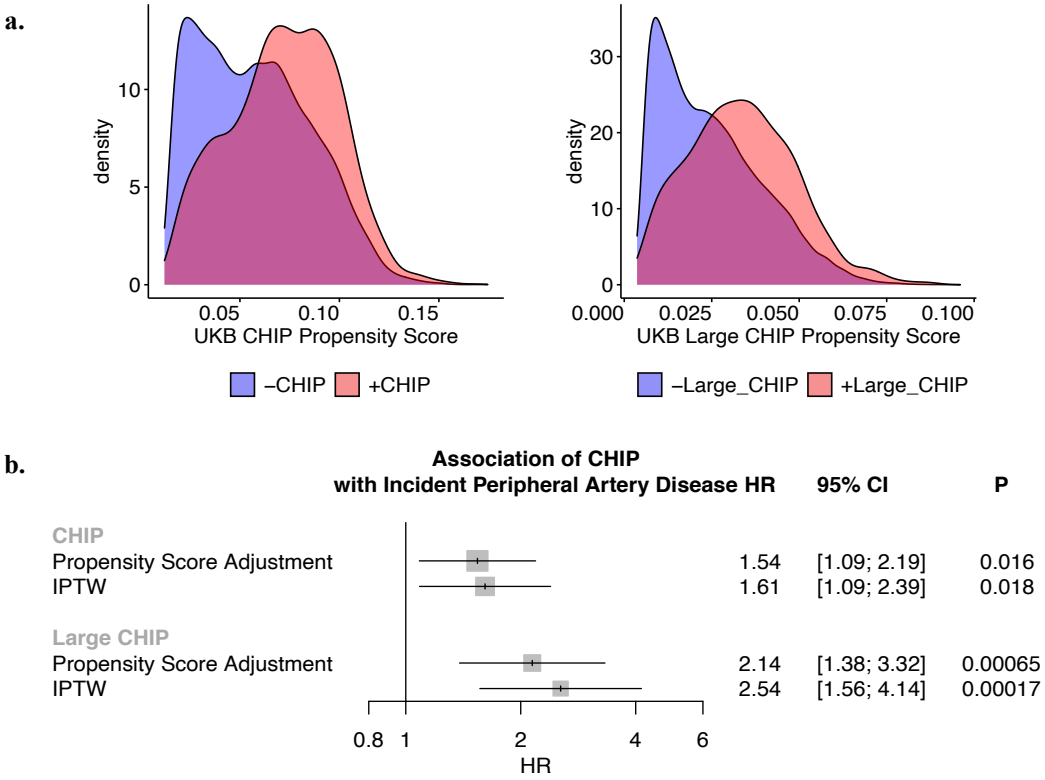

Supplementary Figure V: Epidemiological causal inference analysis for CHIP on incident peripheral artery disease in the UK Biobank. a) Propensity scores by CHIP and Large CHIP status in the UKB. **b)** Propensity score adjustment and stabilized inverse probability treatment weighting (IPTW) for the CHIP and Large CHIP association with incident PAD in the UKB. CHIP = clonal hematopoiesis of indeterminate potential; VAF = variant allele fraction; PAD = peripheral artery disease

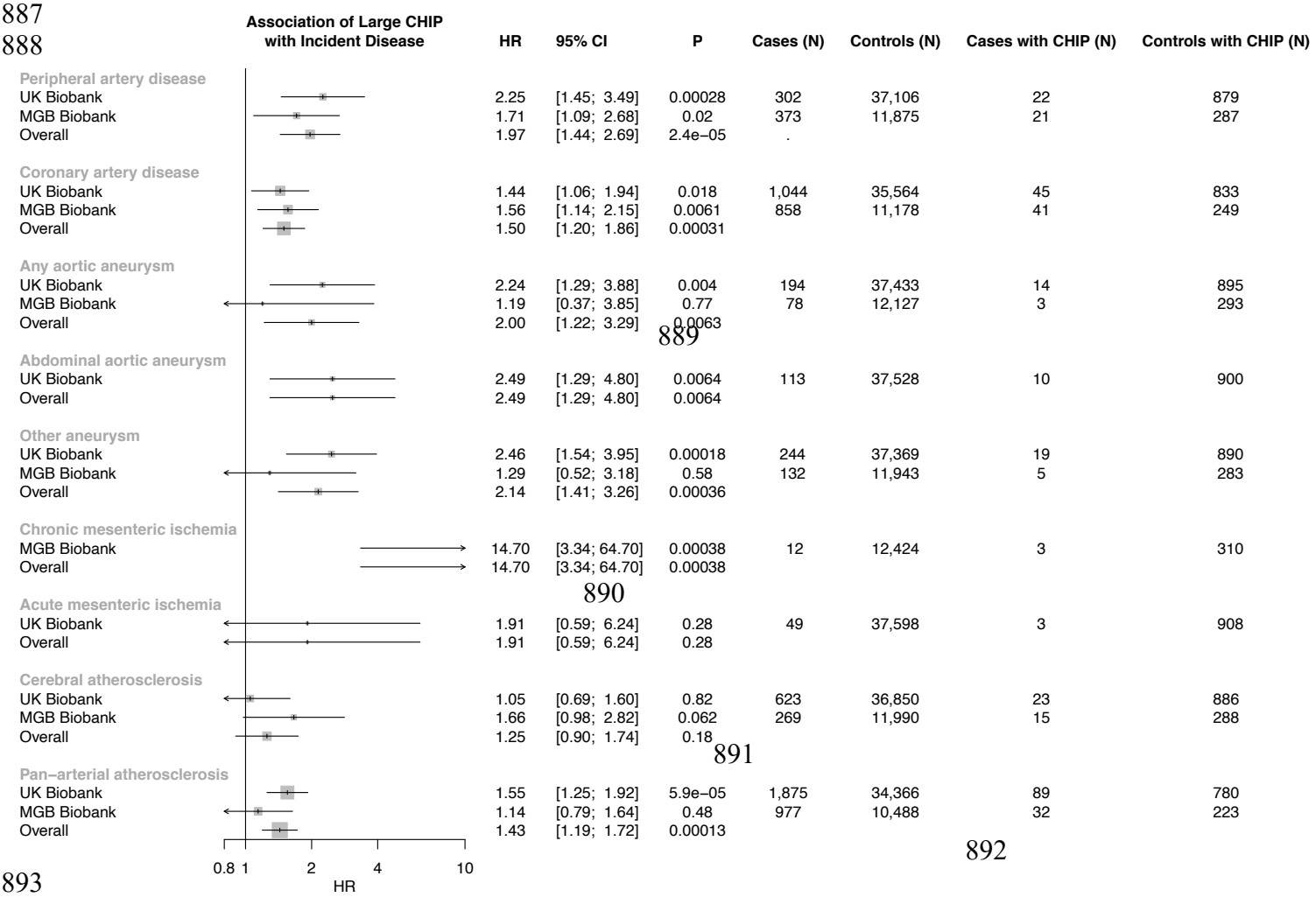

Supplementary Figure VI: Association of Large CHIP (VAF>10%) with incident pan-arterial atherosclerosis, combined across peripheral artery disease, coronary artery disease, aneurysms, chronic and acute mesenteric ischemia, cerebral atherosclerosis, and renal artery stenosis. CHIP = clonal hematopoiesis of indeterminate potential; VAF = variant allele fraction

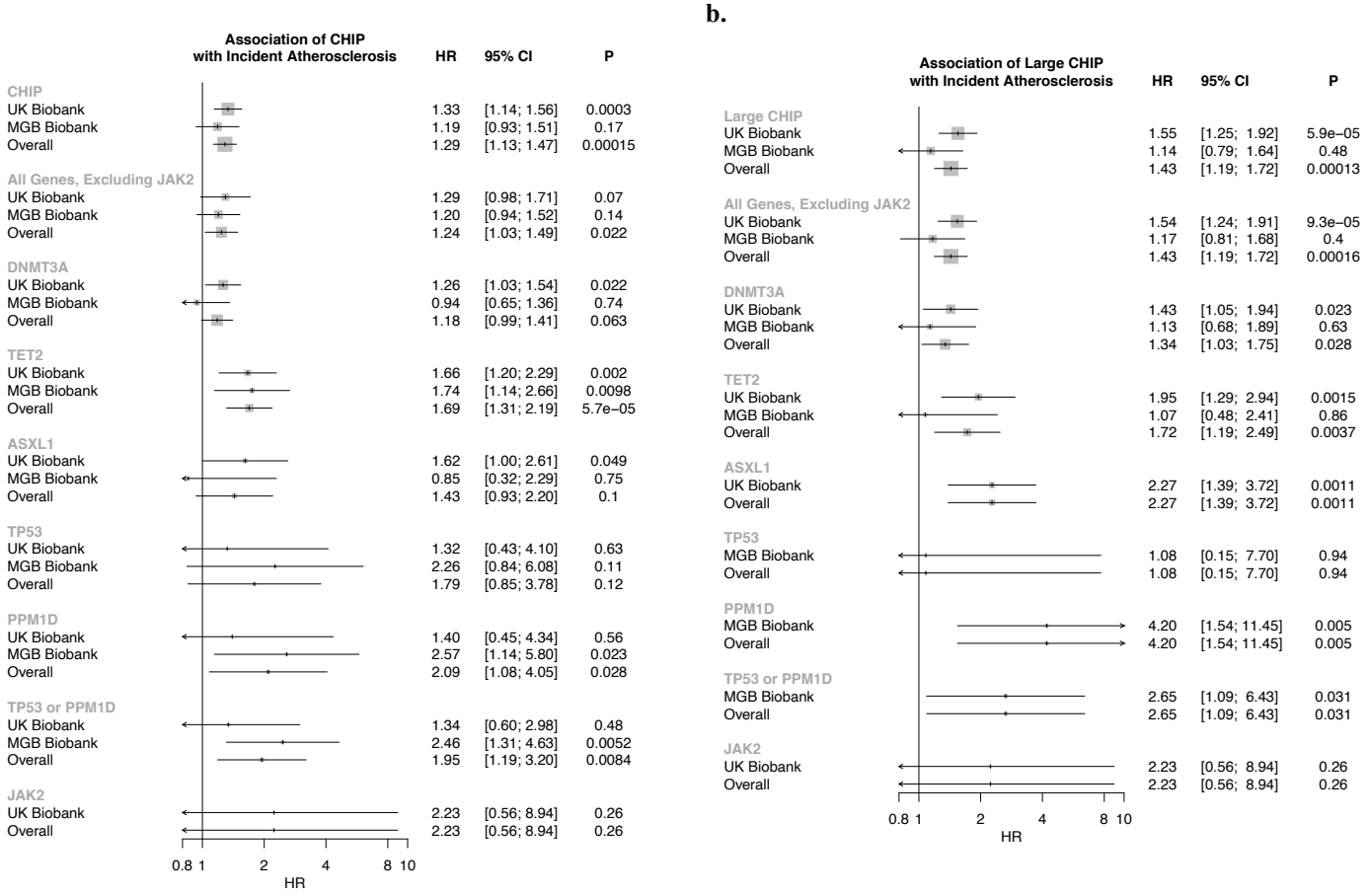

Supplementary Figure VII: Association of **a)** CHIP and **b)** Large CHIP genes with incident pan-arterial atherosclerosis, combined across peripheral artery disease, coronary artery disease, aneurysms, chronic and acute mesenteric ischemia, cerebral atherosclerosis, and renal artery stenosis. CHIP = clonal hematopoiesis of indeterminate potential; VAF = variant allele fraction

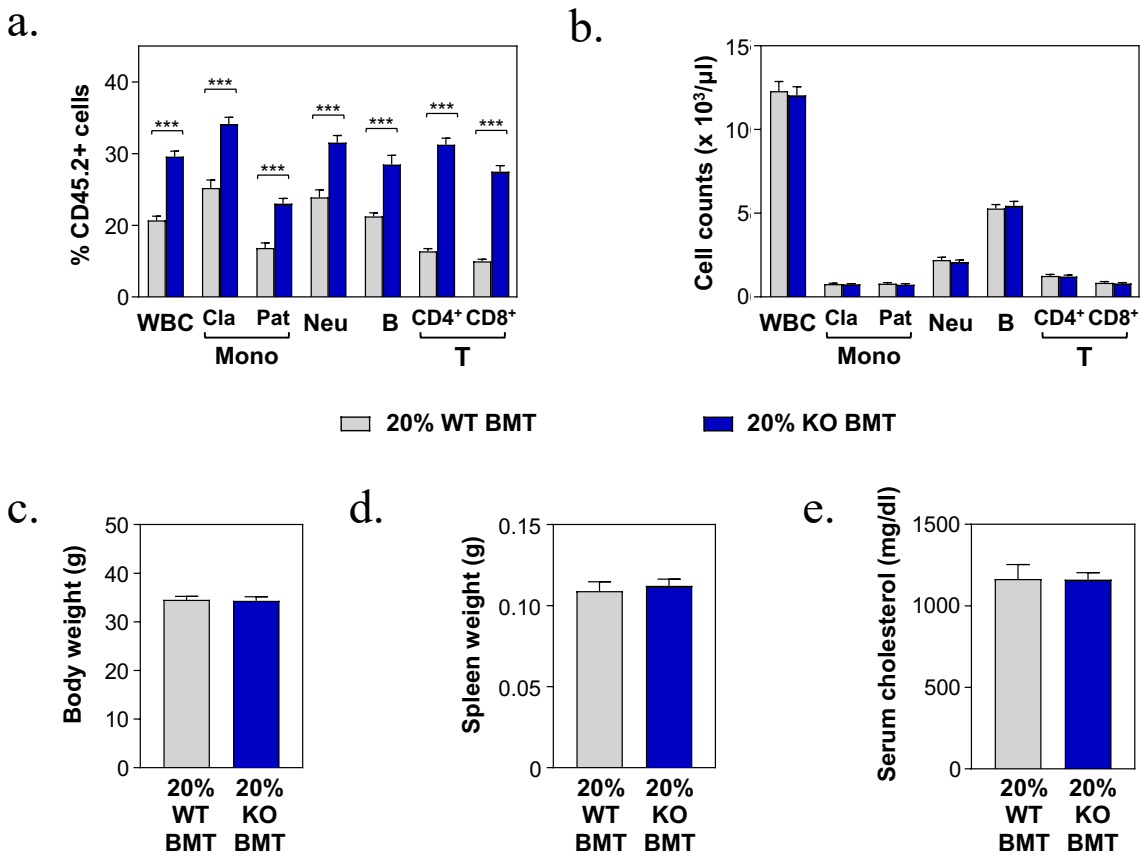

Supplementary Figure VIII: 20% KO-BMT male mice and 20% WT-BMT controls were fed a high-fat/high-cholesterol (HF/HC) diet for 9 weeks, starting 4 weeks after BMT. a) Percentage of CD45.2+ cells in different white blood cell (WBC) lineages in peripheral blood, evaluated by flow cytometry (***p<0.001). b) Absolute counts of main WBC sub-populations in peripheral blood, evaluated by flow cytometry. c) Body weight. d) Spleen weight. e) Total cholesterol level in serum, evaluated by enzymatic methods.

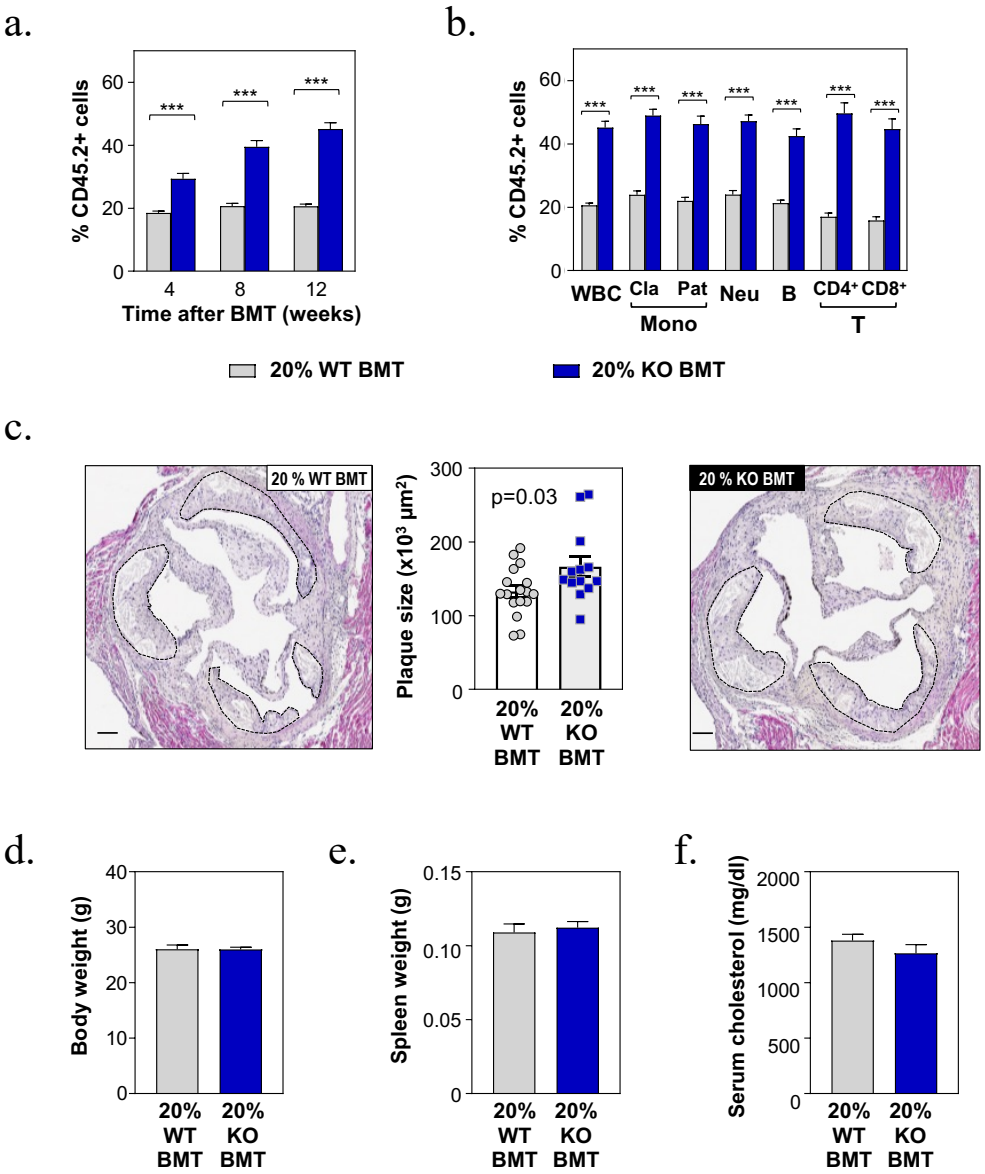

Supplementary Figure IX. 20% KO-BMT female mice (n=13) and 20% WT-BMT controls (n=17) were fed a high-fat/high-cholesterol (HF/HC) diet for 9 weeks, starting 4 weeks after BMT. a) Percentage of CD45.2+ in white blood cells at different timepoints, evaluated by flow cytometry (***p<0.001). b) Percentage of CD45.2+ cells in different white blood cell (WBC) lineages in peripheral blood after 9 weeks on HF/HC diet (13 weeks post-BMT), evaluated by flow cytometry (***p<0.001). c) Aortic root plaque size. Representative images of hematoxylin and eosin-stained sections are shown; atherosclerotic plaques are delineated by dashed lines. Scale bars, 100 µm. d) Body weight. e) Spleen weight. f) Total cholesterol level in serum, evaluated by enzymatic methods.

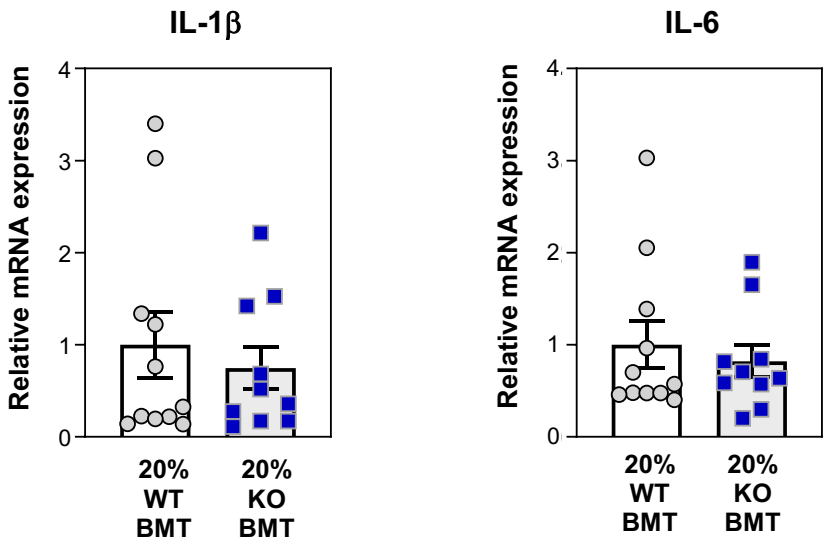

Supplementary Figure X. Aortic arch samples were obtained from HF/HC-fed 20% WT-BMT mice (n=11) or 20% KO-BMT mice (n=10) and gene expression was analyzed by qPCR analysis.

991 **Sources:**

992 1. Conte MS, Bradbury AW, Kolh P, White JV, Dick F, Fitridge R, Mills JL, Ricco JB,
993 Suresh KR and Murad MH. Global vascular guidelines on the management of chronic limb-
994 threatening ischemia. *J Vasc Surg*. 2019;69:3S-125S.e40.
995 2. Jaiswal S, Fontanillas P, Flannick J, Manning A, Grauman PV, Mar BG, Lindsley RC,
996 Mermel CH, Burtt N, Chavez A, et al. Age-Related Clonal Hematopoiesis Associated with
997 Adverse Outcomes. *New England Journal of Medicine*. 2014;371:2488-2498.
998 3. Jaiswal S, Natarajan P, Silver AJ, Gibson CJ, Bick AG, Shvartz E, McConkey M, Gupta
999 N, Gabriel S, Ardissino D, et al. Clonal Hematopoiesis and Risk of Atherosclerotic
1000 Cardiovascular Disease. *New England Journal of Medicine*. 2017;377:111-121.
1001 4. Xie M, Lu C, Wang J, McLellan MD, Johnson KJ, Wendl MC, McMichael JF, Schmidt
1002 HK, Yellapantula V, Miller CA, et al. Age-related mutations associated with clonal
1003 hematopoietic expansion and malignancies. *Nature medicine*. 2014;20:1472-8.
1004 5. Genovese G, Kähler AK, Handsaker RE, Lindberg J, Rose SA, Bakhoum SF, Chambert
1005 K, Mick E, Neale BM, Fromer M, et al. Clonal hematopoiesis and blood-cancer risk inferred
1006 from blood DNA sequence. *N Engl J Med*. 2014;371:2477-87.
1007 6. Bick AG, Pirruccello JP, Griffin GK, Gupta N, Gabriel S, Saleheen D, Libby P,
1008 Kathiresan S and Natarajan P. Genetic Interleukin 6 Signaling Deficiency Attenuates
1009 Cardiovascular Risk in Clonal Hematopoiesis. *Circulation*. 2020;141:124-131.
1010 7. Bycroft C, Freeman C, Petkova D, Band G, Elliott LT, Sharp K, Motyer A, Vukcevic D,
1011 Delaneau O, O'Connell J, et al. The UK Biobank resource with deep phenotyping and genomic
1012 data. *Nature*. 2018;562:203-209.
1013 8. Smoller JW, Karlson EW, Green RC, Kathiresan S, MacArthur DG, Talkowski ME,
1014 Murphy SN and Weiss ST. An eMERGE Clinical Center at Partners Personalized Medicine.
1015 *Journal of personalized medicine*. 2016;6.
1016 9. Van Hout CV, Tachmazidou I, Backman JD, Hoffman JD, Liu D, Pandey AK, Gonzaga-
1017 Jauregui C, Khalid S, Ye B, Banerjee N, et al. Exome sequencing and characterization of 49,960
1018 individuals in the UK Biobank. *Nature*. 2020;586:749-756.
1019 10. Bick AG, Weinstock JS, Nandakumar SK, Fulco CP, Bao EL, Zekavat SM, Szeto MD,
1020 Liao X, Leventhal MJ, Nasser J, et al. Inherited causes of clonal haematopoiesis in 97,691 whole
1021 genomes. *Nature*. 2020;586:763-768.
1022 11. Jaiswal S, Fontanillas P, Flannick J, Manning A, Grauman PV, Mar BG, Lindsley RC,
1023 Mermel CH, Burtt N, Chavez A, et al. Age-related clonal hematopoiesis associated with adverse
1024 outcomes. *N Engl J Med*. 2014;371:2488-98.
1025 12. Jaiswal S, Natarajan P, Silver AJ, Gibson CJ, Bick AG, Shvartz E, McConkey M, Gupta
1026 N, Gabriel S, Ardissino D, et al. Clonal Hematopoiesis and Risk of Atherosclerotic
1027 Cardiovascular Disease. *N Engl J Med*. 2017;377:111-121.
1028 13. Klarin D, Lynch J, Aragam K, Chaffin M, Assimes TL, Huang J, Lee KM, Shao Q,
1029 Huffman JE, Natarajan P, et al. Genome-wide association study of peripheral artery disease in
1030 the Million Veteran Program. *Nature medicine*. 2019;25:1274-1279.
1031 14. Wu P, Gifford A, Meng X, Li X, Campbell H, Varley T, Zhao J, Carroll R, Bastarache L,
1032 Denny JC, et al. Mapping ICD-10 and ICD-10-CM Codes to Phecodes: Workflow Development
1033 and Initial Evaluation. *JMIR Med Inform*. 2019;7:e14325.

1034 15. Zekavat SM, Lin S-H, Bick AG, Liu A, Paruchuri K, Uddin MM, Ye Y, Yu Z, Liu X,
1035 Kamatani Y, et al. Hematopoietic mosaic chromosomal alterations and risk for infection among
1036 767,891 individuals without blood cancer. *medRxiv*. 2020:2020.11.12.20230821.
1037 16. Hernan MA, Brumback B and Robins JM. Marginal structural models to estimate the
1038 causal effect of zidovudine on the survival of HIV-positive men. *Epidemiology*. 2000;11:561-70.
1039 17. Fuster JJ, MacLauchlan S, Zuriaga MA, Polackal MN, Ostriker AC, Chakraborty R, Wu
1040 CL, Sano S, Muralidharan S, Rius C, et al. Clonal hematopoiesis associated with TET2
1041 deficiency accelerates atherosclerosis development in mice. *Science (New York, NY)*.
1042 2017;355:842-847.
1043 18. Fuster JJ, Zuriaga MA, Zorita V, MacLauchlan S, Polackal MN, Viana-Huete V, Ferrer-
1044 Pérez A, Matesanz N, Herrero-Cervera A, Sano S, et al. TET2-Loss-of-Function-Driven Clonal
1045 Hematopoiesis Exacerbates Experimental Insulin Resistance in Aging and Obesity. *Cell reports*.
1046 2020;33:108326.
1047 19. Denny JC, Bastarache L, Ritchie MD, Carroll RJ, Zink R, Mosley JD, Field JR, Pulley
1048 JM, Ramirez AH, Bowton E, et al. Systematic comparison of phenome-wide association study of
1049 electronic medical record data and genome-wide association study data. *Nat Biotechnol*.
1050 2013;31:1102-10.
1051 20. Visconte V, M ON and H JR. Mutations in Splicing Factor Genes in Myeloid
1052 Malignancies: Significance and Impact on Clinical Features. *Cancers (Basel)*. 2019;11.
1053 21. Bondar T and Medzhitov R. p53-mediated hematopoietic stem and progenitor cell
1054 competition. *Cell Stem Cell*. 2010;6:309-22.
1055 22. Liu Y, Elf SE, Miyata Y, Sashida G, Liu Y, Huang G, Di Giandomenico S, Lee JM,
1056 Deblasio A, Menendez S, et al. p53 regulates hematopoietic stem cell quiescence. *Cell Stem Cell*.
1057 2009;4:37-48.
1058 23. TeKippe M, Harrison DE and Chen J. Expansion of hematopoietic stem cell phenotype
1059 and activity in Trp53-null mice. *Exp Hematol*. 2003;31:521-7.
1060 24. Sano S, Oshima K, Wang Y, MacLauchlan S, Katanasaka Y, Sano M, Zuriaga MA,
1061 Yoshiyama M, Goukassian D, Cooper MA, et al. Tet2-Mediated Clonal Hematopoiesis
1062 Accelerates Heart Failure Through a Mechanism Involving the IL-1beta/NLRP3 Inflammasome.
1063 *J Am Coll Cardiol*. 2018;71:875-886.
1064 25. Abplanalp WT, Cremer S, John D, Hoffmann J, Schuhmacher B, Merten M, Rieger MA,
1065 Vasa-Nicotera M, Zeiher AM and Dimmeler S. Clonal Hematopoiesis-Driver DNMT3A
1066 Mutations Alter Immune Cells in Heart Failure. *Circ Res*. 2021;128:216-228.
1067 26. Sinha SK, Miikeda A, Fouladian Z, Mehrabian M, Edillor C, Shih D, Zhou Z, Paul MK,
1068 Charugundla S, Davis RC, et al. Local M-CSF (Macrophage Colony-Stimulating Factor)
1069 Expression Regulates Macrophage Proliferation and Apoptosis in Atherosclerosis. *Arterioscler*
1070 *Thromb Vasc Biol*. 2021;41:220-233.
1071 27. Klarin D, Verma SS, Judy R, Dikilitas O, Wolford BN, Paranjpe I, Levin MG, Pan C,
1072 Tcheandjieu C, Spin JM, et al. Genetic Architecture of Abdominal Aortic Aneurysm in the
1073 Million Veteran Program. *Circulation*. 2020.
1074 28. Shimizu K, Mitchell RN and Libby P. Inflammation and cellular immune responses in
1075 abdominal aortic aneurysms. *Arterioscler Thromb Vasc Biol*. 2006;26:987-94.
1076 29. Boesten LS, Zadelaar AS, van Nieuwkoop A, Hu L, Teunisse AF, Jochemsen AG, Evers
1077 B, van de Water B, Gijbels MJ, van Vlijmen BJ, et al. Macrophage p53 controls macrophage
1078 death in atherosclerotic lesions of apolipoprotein E deficient mice. *Atherosclerosis*.
1079 2009;207:399-404.

1080 30. Fuster JJ, Fernandez P, Gonzalez-Navarro H, Silvestre C, Nabah YN and Andres V.
1081 Control of cell proliferation in atherosclerosis: insights from animal models and human studies.
1082 *Cardiovasc Res*. 2010;86:254-64.
1083 31. Guevara NV, Kim HS, Antonova EI and Chan L. The absence of p53 accelerates
1084 atherosclerosis by increasing cell proliferation in vivo. *Nat Med*. 1999;5:335-9.
1085 32. Mercer J, Figg N, Stoneman V, Braganza D and Bennett MR. Endogenous p53 protects
1086 vascular smooth muscle cells from apoptosis and reduces atherosclerosis in ApoE knockout
1087 mice. *Circ Res*. 2005;96:667-74.
1088 33. Merched AJ, Williams E and Chan L. Macrophage-specific p53 expression plays a
1089 crucial role in atherosclerosis development and plaque remodeling. *Arterioscler Thromb Vasc*
1090 *Biol*. 2003;23:1608-14.
1091 34. Sanz-Gonzalez SM, Barquin L, Garcia-Cao I, Roque M, Gonzalez JM, Fuster JJ, Castells
1092 MT, Flores JM, Serrano M and Andres V. Increased p53 gene dosage reduces neointimal
1093 thickening induced by mechanical injury but has no effect on native atherosclerosis. *Cardiovasc*
1094 *Res*. 2007;75:803-12.
1095 35. van Vlijmen BJ, Gerritsen G, Franken AL, Boesten LS, Kockx MM, Gijbels MJ,
1096 Vierboom MP, van Eck M, van De Water B, van Berkel TJ, et al. Macrophage p53 deficiency
1097 leads to enhanced atherosclerosis in APOE*3-Leiden transgenic mice. *Circ Res*. 2001;88:780-6.
1098 36. Robbins CS, Hilgendorf I, Weber GF, Theurl I, Iwamoto Y, Figueiredo JL, Gorbatov R,
1099 Sukhova GK, Gerhardt LM, Smyth D, et al. Local proliferation dominates lesional macrophage
1100 accumulation in atherosclerosis. *Nat Med*. 2013;19:1166-72.
1101 37. Heyde A, Rohde D, McAlpine CS, Zhang S, Hoyer FF, Gerold JM, Cheek D, Iwamoto
1102 Y, Schloss MJ, Vandoorne K, et al. Increased stem cell proliferation in atherosclerosis
1103 accelerates clonal hematopoiesis. *Cell*. 2021;184:1348-1361 e22.
1104 38. Fidler TP, Xue C, Yalcinkaya M, Hardaway B, Abramowicz S, Xiao T, Liu W, Thomas
1105 DG, Hajebrahimi MA, Pircher J, et al. The AIM2 inflammasome exacerbates atherosclerosis in
1106 clonal haematopoiesis. *Nature*. 2021;592:296-301.
1107